NASA TECHNICAL NOTE

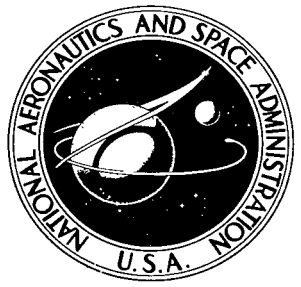

NASA TN D-5899

NASA TN D-5899

HEAT-TRANSFER MEASUREMENTS AT MACH 8 ON A FLAT PLATE WITH DEFLECTED TRAILING-EDGE FLAP WITH EFFECTS OF TRANSITION INCLUDED

by Charles B. Johnson

Langley Research Center
Hampton, Va. 23365

NATIONAL AERONAUTICS AND SPACE ADMINISTRATION • WASHINGTON, D. C. • JULY 1970

1. Report No.	2. Government Accession No.	3. Recipient's Catalog No.
NASA TN D-5899		

4. Title and Subtitle	5. Report Date
HEAT-TRANSFER MEASUREMENTS AT MACH 8 ON A FLAT PLATE WITH DEFLECTED TRAILING-EDGE FLAP WITH EFFECTS OF TRANSITION INCLUDED	July 1970
	6. Performing Organization Code

7. Author(s)	8. Performing Organization Report No.
Charles B. Johnson	L-6349
	10. Work Unit No.
9. Performing Organization Name and Address	129-01-20-07
NASA Langley Research Center Hampton, Va. 23365	11. Contract or Grant No.
	13. Type of Report and Period Covered
12. Sponsoring Agency Name and Address	Technical Note
National Aeronautics and Space Administration Washington, D.C. 20546	14. Sponsoring Agency Code

15. Supplementary Notes

16. Abstract

An experimental heat-transfer investigation was made on a flat-plate model with a short trailing-edge flap deflected at angles of 10°, 20°, and 30° relative to the plate surface. The tests were conducted at a nominal free-stream Mach number of 8, and the nominal free-stream unit Reynolds number was varied from 0.72×10^6 to 35.8×10^6 per meter. The heat-transfer and schlieren results indicated that transition first occurred for the largest flap angle in the separated region at a unit Reynolds number approximately an order of magnitude lower than that for an undisturbed flat plate. Various theories for laminar flow are applied for separated- and attached-flow conditions, and various theories for turbulent flow are applied to the flow over the flap. The heating near flow reattachment on the flap for transitional separation was as much as two times greater than the theoretical prediction for turbulent flow.

17. Key Words (Suggested by Author(s))	18. Distribution Statement
Heat transfer Separated flow	Unclassified – Unlimited

19. Security Classif. (of this report)	20. Security Classif. (of this page)	21. No. of Pages	22. Price*
Unclassified	Unclassified	53	$3.00

*For sale by the Clearinghouse for Federal Scientific and Technical Information
Springfield, Virginia 22151

HEAT-TRANSFER MEASUREMENTS AT MACH 8 ON A FLAT PLATE WITH DEFLECTED TRAILING-EDGE FLAP WITH EFFECTS OF TRANSITION INCLUDED

By Charles B. Johnson
Langley Research Center

SUMMARY

An experimental investigation was made on a flat-plate model with a short trailing-edge flap deflected at angles of 10°, 20°, and 30° relative to the plate surface. These tests were conducted at a nominal free-stream Mach number of 8 and the nominal free-stream unit Reynolds number was varied from 0.72×10^6 to 35.8×10^6 per meter. Heat-transfer measurements and schlieren photographs were obtained at a range of wall-to-total temperature ratio of approximately 0.4 to 0.5. Predictions from several theories for laminar separated and attached flows were compared with data obtained on the plate and flap. Predictions from theories for attached turbulent flow were compared with data obtained on the flap.

The combined results of schlieren photographs and heat-transfer data showed that for the largest flap angle transition occurred over the separated boundary somewhat downstream of the separation point at a unit Reynolds number which is approximately an order of magnitude lower than the unit Reynolds number at which the first indication of transition on the undisturbed flat plate occurred. The low unit Reynolds number for transition over the separated boundary indicates qualitative agreement with the "point-of-inflection criterion," which asserts that velocity profiles with points of inflection are unstable. Increasing the flap angle produced transition in the separated region at a lower unit Reynolds number.

The heat-transfer predictions from flat-plate laminar similar solutions agreed with the data upstream of the interaction region. Some modified theories for laminar separated flow gave heating predictions which agreed with the data on the flap from the hinge line to the point of reattachment for the lower unit Reynolds number conditions. The flat-plate theories for turbulent flow showed agreement with the attached-flow heat-transfer data on the flap for only the highest unit Reynolds number conditions. The peak-heating data downstream of the point of reattachment on the flap for transitional separation was approximately two times greater than theoretical predictions for turbulent flow.

INTRODUCTION

The general problem of separated flows has been of interest for many years. For vehicles traveling at subsonic and low supersonic speeds, external flow separation can affect their aerodynamic performance, whereas engine performance can be severely compromised when flow separation occurs internally. In low-speed flow, the heat transfer is affected to some degree by separation but not seriously. However, the increased heating rates associated with separation at supersonic and hypersonic speeds, particularly in the area of reattachment, are a serious problem, which has received much attention. The basic types of supersonic and hypersonic separated flows that are studied experimentally are generally produced by one of the following simple two-dimensional and/or axisymmetric flows or configurations:

(1) Shock impingement on the boundary layer

(2) Forward facing step or ramp

(3) Rearward facing step or ramp (with extension for reattachment of dividing streamline)

(4) Base flow or afterbody separation (with dividing streamline not reattached to body) leading to the wake flow problem.

(5) Cavity flow

(6) Various types of protuberances which may be regarded locally as combinations of the previously listed items

One of the most widely investigated separated flows is that produced by a forward facing ramp or flap at the trailing edge of a flat plate. This configuration is generally considered to simulate a control surface at the rear of a vehicle. For hypersonic flows, the length of the flap in relation to the upstream length of the flat plate can affect the separation characteristics, the magnitude of the effect being a function of the Mach number and Reynolds number. The flow may be modeled as a basic fluid-mechanics problem when the flap is of sufficient length to allow the flap pressure to approach the inviscid wedge pressure. (See refs. 1, 2, 3, and 4.) The inviscid-wedge-pressure level on the flap is generally reached when flow reattachment occurs well forward of the flap trailing edge. However, a control surface of a flight vehicle is usually short compared with the vehicle length; consequently, separation studies using a short flap are more practical.

It is the purpose of this report to present the results of an experimental heat-transfer investigation on a flat plate with a short trailing-edge flap and to compare these results with predictions from several theoretical methods of calculating heat transfer in the separated- and attached-flow regions over the plate and flap parts of the model. The data were obtained at a nominal Mach number of 8 over a wall-to-total temperature range

of approximately 0.4 to 0.5 for flap angles of 10^{o}, 20^{o}, and 30^{o} and over a unit Reynolds number range of 0.72×10^{6} to 35.80×10^{6} per meter. The results of pressure-distribution and flow-field studies of this investigation have been reported in references 5 and 6.

Previous heat-transfer tests at a nominal Mach number of 8 with a model similar to the one used in this report are presented in references 7 to 13. The data presented herein are unique in the following respects:

(1) The ratio of the highest to lowest Reynolds number presented herein was 50, whereas it was about 5 for previous data.

(2) The heating data in the separated region and on the flap are shown in more detail in the present investigation than in many previous instances.

(3) The variation with unit Reynolds number of the beginning of the interaction and of the separation and reattachment points are presented herein.

(4) The details of the variation of heating with a gradual change in unit Reynolds number are shown over eight increments of unit Reynolds number.

(5) The effects of flap angle and unit Reynolds number on transition in the separated region are shown.

Additional heat-transfer tests on flat-plate—ramp, cone-cylinder-flare and delta-wing models at various Mach numbers are reported in references 1, 2, 3, and 14 to 25. Investigations with other configurations which produce separated flow are reviewed and listed in references 26 to 30.

SYMBOLS

a speed of sound; also velocity profile parameter, $\left[\frac{\partial\left(\overline{U}/\overline{U}_e\right)}{\partial\left(\overline{Y}/\delta_i\right)}\right]_{\overline{Y}=0}$ for attached flow and $\left(\overline{Y}/\delta_i\right)_{f'=0}$ for separated flow

C_F average skin-friction coefficient

C_f local skin-friction coefficient

c_m specific heat of model material

c_p specific heat at constant pressure

f	stream function (see ref. 36)
G	gas constant
h	enthalpy; also used for heat-transfer coefficient in definition of Stanton number
k	thermal conductivity
L	length of flat-plate part of model, 0.254 meter
M	Mach number
m	pressure-gradient parameter (see eq. (17))
N_{Pr}	Prandtl number
$N_{St,e}$	Stanton number, $h/c_p\rho_e u_e$
n	pressure-gradient parameter (see eq. (21))
p	static pressure
q	heat-transfer rate
R	unit free-stream Reynolds number

$R_{e,x} = \rho_e u_e x/\mu_e$

r	recovery factor

$S = \left(h_t/h_{t,e}\right) - 1$

s	Reynolds analogy factor
T	temperature
T'	reference temperature
t	time

$\overline{\underline{U}}$	Stewartson's transformed velocity (see eq. (16))
u	velocity component parallel to surface
$\overline{\underline{X}},\overline{\underline{Y}}$	Stewartson's transformed coordinates
x	coordinate parallel to surface from leading edge
y	coordinate normal to the wall
β	similar solution pressure-gradient parameter (see eq. (22))
γ	ratio of specific heats at constant pressure and volume
δ_i	transformed boundary-layer thickness
δ_t^*	transformed displacement thickness, $\int_0^{\delta_i}\left(S + 1 - \frac{\overline{\underline{U}}}{\overline{\underline{U}}_e}\right)d\overline{\underline{Y}}$
ζ	stagnation enthalpy ratio, $h_t/h_{t,e}$
η	similarity variable (ref. 36)
θ_f	trailing-edge flap angle (positive when flap is deflected upward)
μ	absolute viscosity
ν	coefficient of kinematic viscosity
ρ	density
ρ_m	model material density
τ_m	model material thickness
ϕ	density-viscosity product ratio, $\rho\mu/\rho_w\mu_w$

Subscripts:

aw	adiabatic wall conditions
e	local external conditions
i	incompressible values
o	at beginning of interaction or at hinge line when there is no interaction region
r	reattachment value
s	separation point
T'	evaluated at T'
t	stagnation conditions
th	theoretical
tr	beginning of transition
v	based on distance from virtual origin of turbulent boundary layer
w	wall conditions
ψ	flow deflection angle at edge of shear layer over separated region
∞	free-stream conditions behind oblique shock
*	value at dividing streamline

A prime indicates differentiation with respect to η except when used on T.

APPARATUS AND TEST PROCEDURE

Description of Model

The heat-transfer model used for these tests is shown in figures 1 and 2. The model was made from AISI type 347 stainless steel and had a sharp leading edge about

0.025 mm thick. The leading-edge section used on the heat-transfer model was the same as the one used on a geometrically similar pressure model described in reference 5. The flat-plate part of the model was 0.197 meter wide and 0.25 meter long. A 0.0508-meter-long trailing-edge flap, which may be positioned at angles of 10°, 20°, and 30° relative to the flat-plate surface extends across the back of the model. Tests were also made with a set of upper side plates with sharp leading edges, which extended back from the leading edge at an angle of approximately 6° as shown in figure 1 on a geometrically similar pressure model.

Instrumentation

The instrumentation for the heat-transfer model consists of 30 gage (0.254-mm diameter) thermocouple wire attached to a thin-skin part of the model. (See fig. 2.) The thermocouple junctions were made by spot welding individual thermocouple wires to the inside surface of the model skin. The thin-skin part was fabricated by milling a groove 1.02 cm wide in the 2.54-cm-thick plate as indicated in figure 2. The flap was made from a 0.762-mm stainless-steel plate and was provided with a shield to prevent extraneous heat inputs from the back or bottom side.

Test Procedure and Data Reduction

The tests were conducted in the Langley Mach 8 variable-density hypersonic tunnel. The tunnel operated at a nominal Mach number of 8 over a range of Reynolds number of 0.72×10^6 to 35.80×10^6 per meter. The tunnel stagnation conditions varied from 172.4 kN/m^2 and 594° K to 18.5 MN/m^2 and 817° K for lowest and highest unit Reynolds numbers, respectively. A Mach number calibration of the flow is given in reference 31, and a further description of the facility is given in reference 32. Throughout the tests, the model was set at $\frac{1^{\circ}}{2}$ angle of attack; this angle of attack resulted in a range of local Mach numbers on the plate from about 7.4 to 7.8.

The heat-transfer tests were made with the model initially at room temperature. The model was injected into the tunnel test section from a vacuum chamber which had been evacuated to the test-section-stream static pressure. Approximately 0.05 second was required for the model to leave the chamber and enter the uniform test-flow region, and the heat-transfer data records were started $\frac{1}{2}$ second after the model was positioned in the test section.

The heat-transfer data were obtained from the temperature-time history of each thermocouple as recorded at the rate of 40 points per second on magnetic tape by an analog-to-digital data-recording system. The temperature-time data were used to obtain dT_w/dt in order to find the heat-storage rate in the thin skin of the model from the

following equation:

$$q = \rho_m c_m \tau_m \left(dT_w/dt\right) \tag{1}$$

The temperature-time derivative was taken as the slope of a linear temperature-time variation based on two temperatures evaluated at 1 and 2 seconds after the model was in the test section. The two temperature data points for this slope were calculated from the midpoint of two second-degree polynomials which were curve fits of the 40 recorded data points for each 1-second interval. The data used in these polynomials started at $\frac{1}{2}$ second and $1\frac{1}{2}$ seconds after the model was in the test section. The above linear method was used to reduce the scatter in the low unit Reynolds number (low-heating-rate) data. The scatter in the low-heating-rate data was a result of the electronic "noise" in the data-recording system. The present linear method considerably reduced the scatter in the data as compared with methods used previously (ref. 33, for example). A calculation was made for the condition of maximum longitudinal conduction and the error was found to be less than 1.0 percent.

The experimental heat-transfer coefficient was calculated from the following expression:

$$h = q/\left(T_{aw} - T_w\right) \tag{2}$$

where

$$T_{aw} = r\left(T_t - T_e\right) + T_e \tag{3}$$

and where T_w was taken as the midpoint $\left(\text{at } 1\frac{1}{2} \text{ seconds after model injection}\right)$ of the linear curve fit described previously.

The recovery factor r for the reduction of all the heating data was $\sqrt{N_{Pr}}$, where $N_{Pr} = 0.72$. The calculation of T_{aw} from equation (3) was made for a nominal Mach number of 8 and the measured value of T_t. The laminar value of recovery factor was used for all data reduction because of the uncertainty in the location of the beginning and end of transition.

RESULTS AND DISCUSSION

Transition

The effect of transition on the extent of separation and the pressure levels in the separated region for the same configuration used in the present investigation has been discussed in references 5 and 6.

Schlieren photographs.- Schlieren photographs of the flow-separation model at $T_w/T_t \approx 0.4$ are shown in figure 3. These schlieren photographs were used to determine the approximate location of the beginning of transition on the separated-flow boundary. (Hereafter, the term "transition" will refer to the beginning of transition.) The location of transition was based on two observations:

(1) A change in appearance of the white line over the separated-flow boundary which represents a change in the density gradient at the approximate outer edge of the boundary layer (The validity of using the schlieren technique for finding transition is discussed and substantiated in ref. 16.)

(2) The formation of waves originating from the same area of the outer edge of the shear region where the change in the white line was observed

The schlieren photographs for $\theta_f = 30^o$ gave an indication of transition for all but the lowest unit Reynolds number tests (transition locations are marked in fig. 3(a)); however, in the schlieren photographs for $\theta_f = 10^o$ and 20^o, transition could only be located for one of the higher unit Reynolds numbers.

Flat-plate results.- The flat-plate transition data are shown in figure 4 and in the following table from references 5 and 6 in order to aid in the interpretation and evaluation of the heat transfer and transition results presented in this report. These data were obtained with the heat-transfer model shown in figures 1 and 2 with $\theta_f = 0^o$.

Unit Reynolds number, per meter	Distance from leading edge to beginning of transition, x/L	Local transition Reynolds number
4.79×10^6	Off the model	---------
8.69	0.90	1.99×10^6
11.32	.80	2.30
14.10	.75	2.69
35.80	.55	5.00

The higher level of the $N_{St,e}\sqrt{R_{e,x}}$ data on the flap in figure 4 is due to a slight misalinement in the positioning of the flap relative to the flat-plate part of the model; however, the misalinement should have no effect on the location of transition.

Heat-transfer results.- The results of the heat-transfer study are presented in figures 5 and 6 in terms of Stanton number and in figures 7 and 8 in terms of the ratio of the measured local heating rate to the theoretical laminar heating rate at the beginning of the interaction. Results in these figures are presented for 30^o, 20^o, and 10^o flap angles on the model with and without side plates. The locations of the beginning of interaction x_o were determined from the pressure data on a geometrically similar model presented in references 5 and 6. The separation point x_s and the reattachment point x_r were

determined from surface oil-flow studies also reported and described in references 5 and 6. The results from these previous oil-flow studies indicated that the separated flow always reattached on the flap even for the lowest unit Reynolds numbers. It was pointed out in references 5 and 6 that the extent and type of separation (see ref. 16 for a definition of the types of separation) is dependent on the length of the flap, particularly at the lower unit Reynolds numbers where reattachment is near the trailing edge. However, at the higher unit Reynolds numbers, as the reattachment point moves toward the hinge line and the flow downstream of reattachment becomes fully turbulent, the length of the flap is believed to have no significant effect on the extent of separation. It should be noted that for $R = 35.80 \times 10^6$ per meter at flap angles of 30^o, 20^o, and 10^o and for $R = 14.10 \times 10^6$ per meter at $\theta_f = 10^o$ there was no separation detected by the surface oil-flow tests.

In figure 5(a) for 0.72×10^6 per meter $\leqq R \leqq 8.69 \times 10^6$ per meter and $\theta_f = 30^o$, the Stanton number decreases rapidly downstream of separation and then at a point in the separated region, upstream of the hinge line, it begins to rise. The increase of the heating with x downstream of the minimum heating in the separated region ($R \leqq 8.69 \times 10^6$ per meter in fig. 5(a)) is believed to be associated with the start of transition occurring in the shear layer. (See refs. 15 and 21.) The location of the start of transition in the shear layer based on the rise in heating on the surface of the model ahead of the hinge line for both separated and attached flow is indicated by x_{tr} in figures 5, 6, 7, and 8.

Comparisons of heat-transfer and schlieren results.- The location of transition as indicated by the heat-transfer data and the most upstream location of transition as indicated by the schlieren photographs are compared in figure 9 for $\theta_f = 30^o$ and 20^o. The curves for the separation point and for transition location (fig. 9) have the same trend with change in unit Reynolds number until transition moves upstream of the separation point. The location of transition as indicated by the schlieren photographs is generally downstream of the location indicated by the heat-transfer data possibly because some distance may be required for the structural changes associated with transition in the shear layer to develop sufficiently to be observed in the schlieren pictures. The distance between the start of transition and the separation point for $\theta_f = 30^o$ decreases as the unit Reynolds number increases up to a unit Reynolds number per meter of approximately 10^7. (See fig. 9(a).) The agreement in the trends for the transition location inferred from the heat transfer and schlieren data in figure 9(a) supports the supposition that the rise in heat transfer in figures 5, 6, 7, and 8 is associated with the beginning of transition on the separated-flow boundary.

The data in figures 5(a) and 5(b) at $R = 8.69 \times 10^6$ per meter indicate that the start of transition in the separated shear layer occurs at $x/L = 0.85$ for $\theta_f = 20^o$ and

at $x/L = 0.70$ for $\theta_f = 30^o$. The start of transition on the flat plate $(\theta_f = 0^o)$ for $R = 8.69 \times 10^6$ per meter occurs at $x/L = 0.90$, which is somewhat downstream of the transition point for $\theta_f = 30^o$ and 20^o. Consequently, for a given free-stream unit Reynolds number, the effect of separation is to move the start of transition upstream. An exception to this effect of separation on transition is noted for the data in figure 5(c) at $\theta_f = 10^o$ and $R = 8.69 \times 10^6$ per meter. For this condition, there was no observed increase in the separated region upstream of the hinge line. Based on the heating distribution, transition did not occur in this region. The reason for this anomalous result is not known.

Effect of flap angle and Reynolds number.- The effect of flap angle on transition in the separated region is shown in figures 5 to 9. The $\theta_f = 30^o$ data of figure 5(a) first indicate transition at $R = 0.72 \times 10^6$ per meter, whereas for the $\theta_f = 20^o$ data, transition is first detected at $R = 1.38 \times 10^6$ per meter. Transition in the separated regions for $\theta_f = 10^o$ (fig. 5(c)) apparently did not occur since no increase in heating for $R \leq 8.69 \times 10^6$ per meter was observed. For the $\theta_f = 0^o$ data, transition first occurred at $R = 8.69 \times 10^6$ per meter. Thus the transition on the separated-flow boundary first occurs for the largest flap angles at a unit Reynolds number which is approximately an order of magnitude lower than the unit Reynolds number at which the first indication of transition on an undisturbed flat plate $(\theta_f = 0^o)$ occurs. (Compare figs. 4 and 5(a).) For a given unit Reynolds number, transition was observed to move forward as the flap angle was increased. This forward movement of transition is related to the forward movement of separation as the flap angle is increased. From these results, it appears that transition (probably associated with shear-layer instability) occurs at progressively lower unit Reynolds numbers as the flap angle increases from 10^o to 30^o.

Possible reasons for transition occurring at progressively lower unit Reynolds numbers when θ_f increases are as follows:

(1) The pressure level increases as the flap angle increases in the area of the pressure plateau above the separated region. The increases in pressure-plateau level are noted in practically all studies with a deflected trailing-edge flap and particularly in the experimental and theoretical results of references 5, 6, and 34.

(2) The extent of separation upstream of the hinge line increases as the flap angle increases, as shown in figures 5, 6, 7, and 8. The pressure data upstream of the hinge line in references 5 and 6 indicate that a distinct pressure plateau above the separated shear layer is only formed for long separated regions, for which transition occurs a short distance downstream of separation (see figs. 5, 6, 7, and 8). Apparently, separation is transitional when a well-defined pressure-plateau region is present and is laminar when no pressure plateau is present, as pointed out in reference 34. The results also

imply that if transition is to occur near the point of separation, then the extent of separation must be large.

(3) A final possibility is that the adverse pressure gradient at the point of separation may increase with an increase in the flap angle. The experimental pressure data in references 5 and 6 do not clearly show such an increase in pressure gradient because of the scatter in the data. However, the theoretical results of references 5 and 6 show that at a given unit Reynolds number, larger peak (or plateau) pressure levels were always associated with larger pressure gradients near the separation point. In turn, the larger peak (or plateau) pressure levels were caused by an increase in flap angle. A discussion of boundary-layer stability in reference 35 states that "a favourable pressure gradient stabilizes the flow, whereas an adverse pressure gradient enhances instability." Thus, a decrease in stability with an increase in flap angle may be caused in part by the increase in pressure gradient in the neighborhood of the separation point.

Classification of separation.- The location of the beginning of transition in the separated region for $\theta_f = 30^o$ in figure 5(a) indicates that these separation data are all transitional. The separation data at $R = 14.10 \times 10^6$ per meter (fig. 5(a)) may also be considered transitional, even though transition starts upstream of the separation point, if the end of transition occurs downstream of the point of separation. The flow is completely attached for all three flap angles at $R = 35.80 \times 10^6$ per meter. The data in the separated regions for $\theta_f = 20^o$ (fig. 5(b)) are considered to be representative of laminar separation for $R \leqq 0.95 \times 10^6$ per meter based on the fact that the heating data upstream of the hinge line are either decreasing or nearly constant; the data for 1.38×10^6 per meter $\leqq R \leqq 14.10 \times 10^6$ per meter are transitional. The classification or type of flow within the separated region for $\theta_f = 10^o$ in figure 5(c) is considered to be laminar for all values of unit Reynolds number based again on the fact that upstream of the hinge line no rise in heating occurs. If transition occurred in the separated-flow boundary over the flap, the exact location of transition would be very difficult to determine because of (1) the rapidly changing heat-transfer rate, (2) the short length of the flap, and (3) the flow reattachment which also occurs on the flap.

Heat Transfer

Stanton number data.- The experimental values of Stanton number shown in figures 5 and 6 were based on two sets of edge conditions. These values were calculated from (1) isentropic edge conditions by using the experimental pressure distribution from reference 5 over the entire model and (2) the oblique-shock edge conditions for the flap part of the model only. The location and magnitude of the peak value of Stanton number on the flap depends on which of these two methods was used to reduce the data. For both methods of calculation when $R \geqq 3.48 \times 10^6$ per meter, the peak Stanton number on the

30° flap (fig. 5(a)) occurs slightly downstream of the measured point of reattachment. However, the peak for isentropic edge conditions is closer to the point of reattachment than the peak for oblique-shock edge properties and first appears at $R = 3.48 \times 10^6$ per meter. The peak value of Stanton number, based on isentropic edge properties, on the flap is approximately 23 times the value evaluated by using the theory for laminar flow (ref. 36) on the flat-plate part of the model at the hinge line for $R = 8.69 \times 10^6$ and 14.10×10^6 per meter.

The results in figures 5(b) and 5(c) for the 20° and 10° flap angles, respectively, are similar to the results found in figure 5(a) for the 30° flap angle. Decreasing the flap angle causes (1) a decrease in the level of heating on the flap, (2) a downstream movement of transition, (3) an increase in the unit Reynolds number for the first indication of transition, and (4) a decrease in the extent of separation.

A comparison of the Stanton number data for the model with and without side plates is presented in figure 6 for flap angles of 30°, 20°, and 10° and Reynolds numbers of 1.38×10^6, 3.48×10^6, and 8.69×10^6 per meter for each flap angle. The effect of side plates on the 30° and 20° flaps (figs. 6(a) and 6(b)) for all three unit Reynolds numbers was to increase the extent of the separated-flow region and thereby reduce the heating on the flat-plate part of the model. The extent of the separated-flow region and the heating distribution for the 10° flap data in figure 6(c) were essentially the same as the corresponding data in figure 5(c) for the flap without side plates except at $R = 8.69 \times 10^6$ per meter where the data for isentropic edge conditions are slightly higher for the model with side plates than for that without side plates. The effect of side plates on the level of peak heating on the flap for the 30° and 20° flap angles, as shown in figures 6(a) and 6(b), was as follows:

(1) At $R = 1.38 \times 10^6$ per meter, the data for the model without side plates for both isentropic and oblique-shock edge conditions is higher than the data for the model with side plates.

(2) The data for the model with no side plates which used oblique-shock edge conditions (open squares) at $R = 3.48 \times 10^6$ per meter are higher than the data for the model with side plates (closed squares), whereas the data for the model with no side plates which used the isentropic edge conditions (open circles) are lower than the data for the model with side plates (closed circles).

(3) The data at $R = 8.69 \times 10^6$ per meter which used oblique-shock edge conditions were the same for the model with and without side plates (squares), whereas the data which used isentropic edge conditions was higher for the model with side plates (closed circles) than for that without side plates (open circles).

There was no effect of side plates on the location of transition with the exception of the

data for $\theta_f = 30^o$ at $R = 1.38 \times 10^6$ and 3.48×10^6 per meter where transition for the model with side plates occurred upstream of that for the model without side plates. The location of transition for the remaining data for the model with side plates was approximately the same as for the model without side plates.

Stanton number theory.- The local similarity solutions (zero pressure gradient) of Beckwith and Cohen (ref. 36) were compared with the heating data up to the hinge line in figures 5 and 6. (See appendix.) The agreement of the data and theory is good upstream of the beginning of interaction (x_o). The data in the separated region downstream of x_o fall considerably below the theory until the effects of transition cause a sharp rise in the heating above the laminar theory.

The well-known theories of Monaghan (T' method, ref. 37) and of Van Driest (ref. 38) for turbulent heating on flat plates are used to obtain Stanton number and the results are compared with the heating data over the flap in figures 5 and 6. These two methods gave nearly the same predictions when the same edge conditions and virtual origins were used. The T' method was used with oblique-shock edge conditions and the virtual origin of the turbulent boundary layer at the hinge line, whereas the Van Driest theory was used with isentropic edge conditions and the virtual origin at (1) the hinge line and (2) the leading edge. The details of the calculation used in the theoretical prediction of Stanton number are given in the appendix.

The Monaghan theory (ref. 37), which uses the hinge line as the virtual origin, shows agreement with the data in figure 5 for only $R = 35.80 \times 10^6$ per meter. The Van Driest theory (ref. 38) which uses isentropic edge properties with the hinge line as the virtual origin slightly overpredicts the data for $R = 35.80 \times 10^6$ per meter for $\theta_f = 30^o$ and 20^o and agrees with data for $\theta_f = 10^o$.

The Van Driest theory which uses isentropic edge properties with the leading edge as the virtual origin underpredicts the peak heating and general level of heating on the flap for all turbulent and transitional separation data. (See ref. 16 for classification of separation.) The T' and the Van Driest methods which use the hinge line as the virtual origin underpredict the peak heating on the flap for $\theta_f = 30^o$ and 20^o for transitional separation at 3.48×10^6 per meter $\leqq R \leqq 14.10 \times 10^6$ per meter. (See fig. 5.) The T' method for a given x/L underpredicts the peak heating on the flap by as much as a factor of three for transitional separation at $\theta_f = 30^o$ (fig. 5(a)). The Van Driest method with the hinge line as the virtual origin and with measured pressures for $R = 8.69 \times 10^6$ and 14.10×10^6 per meter shows closer agreement with the data on the downstream part of the flap than the T' method does. Thus, it appears that the use of isentropic edge conditions with measured pressure will give a closer prediction of the level of heating in the downstream part of the flap than the use of the oblique-shock edge conditions. The data on the flap in figure 5(b) for $\theta_f = 20^o$ at $R \leqq 0.95 \times 10^6$ per meter

and in figure 5(c) for $\theta_f = 10^o$ at $R \leqq 4.79 \times 10^6$ per meter are overpredicted by both methods which use the hinge line as the virtual origin. These data which are overpredicted by the two methods using the hinge line as the virtual origin show no indication of transition in the separated region upstream of the hinge line.

Heating-rate data.- The heat-transfer data in figures 7 and 8 are presented as the ratio of the local heat-transfer rate q to the theoretical flat-plate heat-transfer rate at the beginning of the interaction region $q_{th,o}$. For the data at $R = 35.80 \times 10^6$ per meter, there was no interaction region and $q_{th,o}$ was evaluated at the hinge line. These are the same data as presented in figures 5 and 6, but are presented in terms of the nondimensional heating rate $q/q_{th,o}$ for the following reasons: (1) The basic interest and application of the experimental data to design problems is generally in terms of heating rates; (2) the recovery temperature is not required; and (3) several of the theories applicable to separated flows are more readily calculated in terms of $q/q_{th,o}$.

As a result of presenting the data in terms of $q/q_{th,o}$, the following conclusions are noted:

(1) The $q/q_{th,o}$ ratio on the 30^o flap in figure 7(a) for $R \geqq 4.79 \times 10^6$ per meter is nearly constant after the peak value is reached.

(2) For 4.79×10^6 per meter $\leqq R \leqq 14.10 \times 10^6$ per meter, the nearly constant value of heating on the 30^o flap is approximately 40 times the laminar heating rate at the beginning of the interaction on the flat-plate part of the model; however, the heating rate on the 30^o flap for $R = 35.80 \times 10^6$ per meter is only about 30 times the theoretical laminar reference value. (See fig. 7(a).) These results indicate again that transitional separation causes higher heating rates on the flap than turbulent attached flow.

(3) The 20^o flap heating data in figure 7(b) for $R = 8.69 \times 10^6$ per meter and $R = 14.10 \times 10^6$ per meter have a constant value of heating rate after reattachement that is approximately 30 times the laminar flat-plate value at the beginning of the interaction. The heating on the 20^o flap for $R = 35.80 \times 10^6$ per meter is also constant along the flap and is approximately 23 times the theoretical laminar flat-plate value at the hinge line.

(4) The 10^o flap data in figure 7(c) for $R \geqq 8.69 \times 10^6$ per meter again show the nearly constant values of heating after reattachment with heating ratios of approximately 15 times the laminar reference values.

A comparison of the heating-rate data for the model with and without side plates is presented in figure 8 for flap angles of 30^o, 20^o, and 10^o and Reynolds numbers of 1.38×10^6, 3.48×10^6, and 8.69×10^6 per meter for each flap angle. On the flap, all the data for the model with side plates for $\theta_f = 10^o$ and the data for $\theta_f = 30^o$ and 20^o at $R = 8.69 \times 10^6$ per meter are approximately the same as the corresponding data for the

model without side plates. The data on the flap for the model with side plates for $\theta_f = 30^o$ and 20^o at $R = 1.38 \times 10^6$ and 3.48×10^6 per meter show a lower level of heating than the data for the model with no side plates. In general, the level of heating in the separation region upstream of the hinge line is lower for all the side-plate data.

Heating-rate theory.- Chapman (ref. 39) has predicted that the value of the average heat flux to the wall in a separated region for laminar flow is reduced by a factor of 0.56 of the value for attached flat-plate flow. The average heat input from the separation point to the hinge line for the data at $\theta_f = 20^o$ and $R = 0.72 \times 10^6$ and 0.95×10^6 per meter in figure 7(b) is approximately 0.50 and 0.61 of the undisturbed flat-plate value, respectively. These measured values are within 11 percent of the Chapman factor.

The first quantitative analysis of a separated flow field was the integral analysis of Lees and Reeves (ref. 40). This method may be adapted for the prediction of the heating distributions in separated flows. (See appendix.) The method of determining the initial conditions used in the calculation of pressure distribution and the resulting pressure distributions from the Lees and Reeves theory are presented in references 5 and 6 from the beginning of the interaction to the hinge line for $\theta_f = 30^o$, 20^o, and 10^o. The heat-transfer predictions which were calculated as a part of the above pressure distributions are presented in figures 7 and 8 and are referred to as the Lees and Reeves I theory. A modification was made to the method of determining the initial conditions used in the Lees and Reeves theory in order to obtain a solution over the flap. (See appendix.) The heat-transfer theory using this modification is referred to as Lees and Reeves II theory. The results from this theory are compared with the $\theta_f = 10^o$ data in figures 7(c) and 8(c) from the beginning of the interaction to the point of reattachment. In general, the Lees and Reeves I theory tends to overpredict the heating in the separated region upstream of the hinge line (or upstream of transition) until the effects of transition at $\theta_f = 30^o$ and 20^o increase the level of heating, as shown in figures 7(a) and 7(b). In figure 7(c) for $\theta_f = 10^o$, both the Lees and Reeves I and the Lees and Reeves II theories are shown. The Lees and Reeves II theory gives closer agreement with the data in the separated flow region than the Lees and Reeves I theory; however, the Lees and Reeves II theory still slightly overpredicts the heating in the separated region over the flat-plate part of the model and underpredicts the heating on the flap. For laminar separation at $R = 0.72 \times 10^6$ per meter in figure 7(c), the Lees and Reeves II theory gives a close representation of the heating on the flap, but for $R \geq 0.95 \times 10^6$ per meter the Lees and Reeves II theory on the flap underpredicts the data by an increasing amount with an increase in the unit Reynolds number. Solutions on the flap were possible only when the extent of separation was small. This small extent of flow separation occurs on the model without side plates for the 10^o flap angle. A solution was obtained for this model at $R = 3.48 \times 10^6$ per meter (fig. 7(c)); however, no solution could be obtained for the model

with side plates at the same θ_f and R because of the increase in the extent of separation caused by the side plates.

The laminar theory of Bertram and Feller (ref. 41, see appendix) may also be used to calculate heat transfer in a separated region; however, prior knowledge of the pressure distribution is required. The theoretical results shown in figures 7 and 8 were calculated by using the experimental pressures over the flap; the theory predicted the heating distribution reasonably well upstream of reattachment for $R \leqq 3.48 \times 10^6$ per meter for the 30^o and 20^o flap angles. (See figs. 7(a) and 7(b).) For the higher unit Reynolds numbers and for the data downstream of reattachment, the Bertram and Feller theory underpredicts the data.

The modified separation-flow theory of Bushnell (ref. 42), in which the experimental separated flow geometry from schlieren photographs and oil flows is used (see appendix), is applied to flat-plate—trailing-edge-flap configuration, and the results are compared with the data on the flap in figures 7 and 8. The trend with unit Reynolds number from this theory is similar to the trend of the Bertram and Feller theory. The Bushnell theory predicts the heating from the hinge line to a point somewhat upstream of the reattachment point at $\theta_f = 30^o$ and 20^o and $R \leqq 3.48 \times 10^6$ per meter. As the unit Reynolds number increases, the extent of the prediction over the flap is reduced. The irregularities in the theoretical curves for $\theta_f = 10^o$ from the Bertram and Feller (ref. 41) method over the flap in figure 7(c) are due to the use of the experimental value of the pressure distribution in the calculation.

CONCLUDING REMARKS

General Conclusions From Data

Heat-transfer tests were conducted on a flat-plate model with a relatively short trailing-edge flap. The length of the flap may have affected the extent of separation, particularly at the lower unit Reynolds number R, where reattachment was near the trailing edge of the flap. The heat-transfer and schlieren results suggest that the rise of heat transfer in the separated region over the flat-plate part of the model is associated with the beginning of transition on the separated-flow boundary. This transition on the separated-flow boundary first occurs for the largest flap angles at a unit Reynolds number which is approximately an order of magnitude lower than the unit Reynolds number at which the first indication of transition on an undisturbed flat plate occurs. For a given unit Reynolds number, transition was observed to move forward as the flap angle was increased. This forward movement of transition is related to the forward movement of separation as the flap angle is increased.

There was no separation at a unit Reynolds number of 35.80×10^6 per meter for the 30^o and 20^o flap angles and no separation for Reynolds numbers of 14.10×10^6 and 35.80×10^6 per meter for the 10^o flap angle. The classification of the type of separation for the data with no side plates based on the heating variations upstream of the hinge line is as follows: (1) the data for a flap angle of 30^o appear to be transitional; (2) the data for a flap angle of 20^o are transitional for a Reynolds number between 1.38×10^6 to 14.10×10^6 per meter; and (3) all the data for a flap angle of 10^o appear to be laminar.

The schlieren photographs and the distribution of the heat transfer for the 30^o flap angle indicated that as the unit Reynolds number was increased from 0.72×10^6 to 35.80×10^6 per meter the distance between the transition point and separation point decreased.

The peak heating rate on the flap for separated flows was as much as 40 times the reference flat-plate value for the highest unit Reynolds number and the largest flap angle. In general, the heating on the flap increased with increasing flap angle.

Conclusions From Comparison of Data With Theories

Stanton number theories.- Various heat-transfer theories for the prediction of Stanton number were evaluated with the following results:

1. The local similarity theory for laminar boundary layers of Beckwith and Cohen predicts reasonably well the flat-plate heating upstream of the beginning of the interaction.

2. The Beckwith and Cohen theory overpredicts the heating in the region of separated flows over the flat-plate part of the model up to the transition location; downstream of transition the theory underpredicts the data.

3. The Monaghan T' and the Van Driest methods with the virtual origin at the hinge line predict reasonably well the turbulent heating on the flap for attached flow at all three flap deflection angles for the highest unit Reynolds numbers.

4. The peak heating on the flap with transitional separation for flap angles of 30^o and 20^o is underpredicted by both the Monaghan T' and the Van Driest theories at a Reynolds number between 3.48×10^6 and 14.10×10^6 per meter. The T' method for a flap angle of 30^o underpredicts the peak heating on the flap by as much as a factor of three.

5. For transitional separation the use of the measured pressures for calculating the isentropic edge properties resulted in better agreement between data and theory on the flap part of the model than the use of oblique-shock edge properties.

Heating-rate theory.- The theoretical prediction of the heating in terms of the ratio of the local heat-transfer rate to the theoretical flat-plate heat-transfer rate at the beginning of the interaction region was investigated for three laminar theories with the following results:

1. The Lees and Reeves method for separated laminar flows overpredicted the heating in the region of separation over the flat-plate part of the model until effects of transition at flap angles of 30° and 20° increased the level of heating.

2. Solutions for the laminar heating on the flap by the Lees and Reeves method were only possible when the extent of separation was small. This small extent of flow separation occurs on the model without side plates for the 10° flap angle. The theory of Lees and Reeves underpredicted the data on the 10° flap for even the lower unit Reynolds number, and the extent of underprediction increased as the unit Reynolds number increased.

3. The theory of Bertram and Feller in which experimental pressures were used, predicted the heating on the 30° and 20° flaps upstream of reattachment at the five lowest unit Reynolds numbers. The theory underpredicts the heating downstream of reattachment for the lower unit Reynolds numbers, whereas for higher unit Reynolds numbers with transitional separation, the theory underpredicts the data over the entire flap.

4. The modified separation-flow theory of Bushnell, in which the experimental separated-flow geometry from schlieren pictures and oil flows is used, predicted the heating on the flap from the hinge line to upstream of the reattachment point for the lower unit Reynolds numbers. When the unit Reynolds number was increased, the theory of Bushnell underpredicted the data.

Langley Research Center,
National Aeronautics and Space Administration,
Hampton, Va., April 21, 1970.

APPENDIX

METHODS USED FOR CALCULATING HEAT TRANSFER

Laminar Flat-Plate Method

The similar solutions of Beckwith and Cohen (ref. 36) were used to calculate the laminar value of $N_{St,e}$ for the undisturbed flat plate. The expression for the product of the Stanton number and square root of the Reynolds number for $\beta = 0$, c_p constant, and $N_{Pr} = 0.72$ is

$$N_{St,e}\sqrt{R_{e,x}} = \frac{0.982\zeta'_w}{\left(\frac{T_{aw}}{T_t} - \frac{T_w}{T_t}\right)\sqrt{\frac{\rho_e \mu_e}{\rho_w \mu_w}}} \tag{4}$$

The results of the similar solutions are shown in figure 10 in terms of the heat-transfer parameter as a function of the ratio of the temperature at the edge of the boundary layer to the total temperature. The experimental data presented herein have an approximate range of $0.075 \leqq T_e/T_t \leqq 0.084$. The variation of $N_{St,e}\sqrt{R_{e,x}}$ from the mean of the data over the range of experimental conditions is approximately 3 percent, which means that the flat-plate heat-transfer parameter may be treated as a constant for these tests.

In figures 7 and 8, the value of the measured local heating rate q is divided by the theoretical flat-plate laminar heating rate $q_{th,o}$ evaluated at the beginning of the interaction, $(x/L)_o$. This theoretical heating rate is determined by first calculating the theoretical heat-transfer coefficient from the $N_{St,e}\sqrt{R_{e,x}}$ data in figure 10 by using the edge properties calculated with the isentropic-flow assumption and measured pressure distribution (c_p constant). This theoretical heat-transfer coefficient, the measured wall temperature, the measured total temperature with a 0.85 recovery factor r are then used to calculate $q_{th,o}$.

The values for $q_{th,o}$ for all three flap angles at $R = 35.80 \times 10^6$ per meter were evaluated at the hinge line $(x/L = 1.0)$. The actual values of $q_{th,o}$ used to normalize the measured heating rate in figure 5 are listed in the following table:

R, per meter	Value of $q_{th,o}$, kW/m^2, for –		
	$\theta_f = 10^o$	$\theta_f = 20^o$	$\theta_f = 30^o$
	No side plates		
0.72×10^6	0.5314	0.6844	0.7785
.95	.6713	.9136	1.1020
1.38	1.0912	1.1452	1.2427
2.13	1.4277	1.7922	2.1179
3.48	2.1567	2.4493	3.2336
4.79	2.6196	2.8034	3.4379
8.69	3.7477	3.8757	4.3459
14.10	4.7466	4.7443	5.2811
35.80	8.8995	8.9676	8.7656
	Side plates		
1.38×10^6	1.0260	1.3416	1.5254
3.48	2.1156	2.7512	3.4413
8.69	3.7444	4.0440	4.3221

The ratio of $q/q_{th,o}$ for constant flat-plate edge and wall conditions, given by

$$q/q_{th,o} = \sqrt{x_o/x} \tag{5}$$

was derived from equation (4) for attached flow with constant edge and wall conditions.

Turbulent Flat-Plate Method

The Monaghan T' method (ref. 37) and Van Driest theory (ref. 38) for the calculation of turbulent-boundary-layer heat transfer were used to calculate Stanton number on the flap. The Monaghan T' method uses an intermediate temperature derived from the expression for mean enthalpy in reference 37 and defined as

$$T' = 0.54T_w + T_e\left(0.46 + 0.0284M_e^2\right) \tag{6}$$

to evaluate the fluid properties of density and viscosity. The following incompressible Kármán-Schoenherr equations (see ref. 43):

$$\left.\begin{aligned} \frac{0.242}{\sqrt{C_{F,T'}}} &= \log\left(C_{F,T'}R_{v,T'}\right) \\ \frac{C_{fi,T'}}{C_{Fi,T'}} &= \frac{1}{1 + 3.59\sqrt{C_{Fi,T'}}} \end{aligned}\right\} \tag{7}$$

and

are used to obtain a local skin friction in terms of the T' fluid properties. The skin friction based on reference conditions is put into the physical plane by replacing the T' density with the oblique-shock density. The x distance used in the T' reference Reynolds number is based on the virtual origin of the turbulent flow occurring at the hinge line of the plate and flap. The hinge line virtual origin was first postulated by Becker and Korycinski (ref. 21) and used again by Holloway, Sterrett, and Creekmore in reference 15. The Stanton number is calculated from a modified form of the Reynolds analogy,

$$N_{St,e} = \frac{1}{s}\frac{C_f}{2} \tag{8}$$

where s is the Reynolds analogy factor taken from the formulation of Van Driest in reference 38. The variation of s, calculated by using the Van Driest local-skin-friction expression, with the Von Kármán mixing length (see ref. 38) is from approximately 0.823 to 0.833 for a $R_{e,x}$ range from 10^6 to 10^8, respectively. In view of the small change in s over two orders of magnitude in $R_{e,x}$ the value of s used in equation (8) was taken as a constant equal to 0.83 for all calculations using the Reynolds analogy.

The Van Driest method of obtaining Stanton number uses the local value of skin friction obtained from the following equation (ref. 38):

$$\frac{0.242}{\sqrt{C_f\left(\frac{\gamma - 1}{2} M_e^2\right)}}\left(\sin^{-1}\alpha + \sin^{-1}\beta\right) = 0.41 + \log\left(R_{e,x}C_f\right) - 0.76 \log \frac{T_w}{T_e} \tag{9}$$

where

$$\alpha = \frac{2A^2 - B}{\sqrt{B^2 + 4A^2}} \qquad \beta = \frac{B}{\sqrt{B^2 + 4A^2}}$$

$$A^2 = \frac{\frac{\gamma - 1}{2} M_e^2}{T_w/T_e} \qquad B = \frac{1 + \frac{\gamma - 1}{2} M_e}{T_w/T_e} - 1$$

The Reynolds analogy (eq. (8)) is then used to calculate the heat transfer. The Van Driest skin-friction equation (eq. (9)) was solved by transforming it into a form similar to Von Kármán's incompressible local skin-friction equation (see refs. 43 and 44), solving for the transformed local skin friction, and then transforming it back to the physical plane for the local value of skin friction. The edge properties used in the Van Driest local skin friction were evaluated from the measured pressure distribution with the assumption that the compression over the model occurred through a series of weak waves rather than a few strong shocks. This assumption enabled the following expressions to be used to calculate the "isentropic edge conditions" ($\gamma = 1.4$):

$$M_e = \sqrt{\left(\frac{p}{p_\infty}\right)^{-2/7}\left(5.0 + M_\infty^2\right) - 5.0} \tag{10}$$

$$\frac{T_e}{T_\infty} = \frac{5.0 + M_\infty^2}{5.0 + M_e^2} \tag{11}$$

$$u_e = M_e 49.1\sqrt{T_e} \tag{12}$$

Equations (10) to (12) are also used in the reduction of experimental data when "isentropic edge conditions" are used in calculating the experimental Stanton number.

The two applications of the Van Driest method shown in figures 5 and 6 differ in the choice of the virtual origin used in calculating the local Reynolds number. One Van Driest method uses the hinge line as the virtual origin of the flow, the same as used in the Monaghan T' method, whereas the other method used the leading edge as the virtual origin.

Lees and Reeves Method for Separated Flow

Calculations using the Lees and Reeves method for obtaining pressure distributions over the flat-plate part of the model are compared with the data and are discussed in references 5, 6, and 40. In reference 6, an extension of the Lees and Reeves method to include the slope of the enthalpy at the wall ζ'_w and the pressure-gradient parameter m as functions of the Lees and Reeves parameter "a" enabled heat transfer to be calculated at the same time the pressure distributions were being calculated. These heat-transfer solutions are presented in figures 7 and 8 as Lees and Reeves I and are only calculated from the beginning of the interaction to the hinge line. The enthalpy and velocity profiles were calculated by local similarity solutions for $T_w/T_t = 0.6$, $N_{Pr} = 1$, and c_p constant. A polynomial of ζ'_w as a function of the single parameter "a" is given in references 5 and 6 for both separated and attached flows.

The heat-transfer expression is derived from the basic definition of heat transfer to the wall, which is

$$q_w = k_w \frac{\partial T_w}{\partial y_w} \tag{13}$$

By using the Stewartson transformation,

$$d\bar{X} = \frac{p_e a_e}{p_\infty a_\infty} dx \qquad \text{and} \qquad d\bar{Y} = \frac{a_e \rho_e}{a_\infty \rho_\infty} dy \tag{14}$$

with the enthalpy function defined as

$$S_w = \frac{h_{t,w}}{h_{t,e}} - 1 \tag{15}$$

the longitudinal velocity defined as

$$\bar{U} = \frac{a_\infty}{a_e} u \tag{16}$$

and

$$\eta = \bar{Y} \sqrt{\frac{(m+1)}{2} \frac{\bar{U}_e}{\gamma_o \bar{X}}} \tag{17}$$

where

$$m = \frac{\beta}{2 - \beta}$$

the heat-transfer expression is obtained as

$$q_w = \frac{k_w p_e}{\rho_\infty G} \sqrt{\frac{(m+1)}{2} \bar{U}_e \left(\frac{T_e}{T_\infty}\right) \frac{\rho_t}{\mu_t \bar{X}}} \left(\frac{\zeta'_w}{S_w + 1}\right) \tag{18}$$

The ζ'_w and m, which are substituted into equation (18), are plotted as functions of the Lees and Reeves parameter a in figures 11 and 12, respectively. The dimensionless longitudinal distance x/L for flat-plate conditions is transformed to the $\bar{X}$ plane (see eq. (14)) for Reynolds numbers up to 14.10×10^6 per meter. The $\bar{X}$ values in figure 13 are used to determine the $\bar{X}_o$ value at the point where the Lees and Reeves solution joins the upstream flat-plate boundary layer. The $\bar{X}_o$ value is found by using the experimental value of $(x/L)_o$. (See ref. 5.) Once the value of $\bar{X}_o$ is known, the variation of $\bar{X}$, used in equation (18) is found from the integration of Lees and Reeves differential equations.

Determination of the initial conditions used in the Lees and Reeves I theory was accomplished by matching the momentum thickness with the upstream flow at $(x/L)_o$.

(See ref. 5.) The theory predicted pressure distributions upstream of the hinge line which agreed with the data in references 5 and 6. However, the Lees and Reeves I method of calculation was deficient in the following areas: (1) the distance $\left[(x/L)_s - (x/L)_o\right]$ did not agree with the experimental values, (2) the calculated heat transfer overpredicted the data, and (3) a solution over the flap was not found.

In order to obtain a solution over the flap and to improve the heat-transfer predictions, the Lees and Reeves II method for obtaining the initial conditions used in the theory was devised. The Lees and Reeves II method used the initial theoretical value of $\left[(x/L)_s - (x/L)_o\right]$ which were close to the known experimental values. A solution using the Lees and Reeves II method from the beginning of the interaction to the point of reattachment was obtained by first obtaining a solution for the attached and separated regions upstream of the hinge line until the correct value of $\left[(x/L)_s - (x/L)_o\right]$ was found. Then the correct hinge-line location was put into the program and the calculation proceeded into the separated region downstream of the hinge line. The criterion for obtaining a solution in the separated region over the flap is a modification of the method of reference 40 and consists of an iteration for the correct value of M_{∞_+} based on the condition that $\left(0 < N_3 < 0.1\right)$ just downstream of reattachment. This new criterion for establishing the value of M_{∞_+} was based on the assumption that the "neck" in the $\delta_t^* - \underline{\overline{X}}$ plane occurred just downstream of reattachment and satisfied the condition that

$$\frac{d\delta_t^*}{d\underline{\overline{X}}} = \frac{1}{R_{e,\delta_t^*}} \frac{N_3}{D} \approx 0 \tag{19}$$

where

D variable defined by equation (25a) in reference 33

N_3 variable defined by equation (25d) in reference 33

$$R_{e,\delta_t^*} = \frac{a_\infty M_e \delta_t^*}{\nu_\infty}$$

and where R_{e,δ_t^*} and D are finite.

The distance of separated flow from the hinge line to the area of reattachment calculated by the Lees and Reeves II theory compared favorably with the data for $\theta_f = 10^o$. For the data at $\theta_f = 10^o$ at unit Reynolds numbers of 0.72×10^6 and 0.95×10^6 per meter, the distances measured by using surface oil flow from the hinge line to the point of reattachment were 4.72 and 4.60 cm, respectively, while the calculated distances for

the same conditions were 4.52 and 4.45 cm. A solution over the flap, using the Lees and Reeves II theory, could only be obtained when the extent of separation was small. This small extent of separation occurs when $\theta_f = 10^o$.

For instance, at a unit Reynolds number of $R = 3.48 \times 10^6$ per meter, the Lees and Reeves II method converged on a value of M_{∞_+} when the distance from x_o to the hinge line (approximately 4.8 cm corresponded to that for the model without side plates and $\theta_f = 10^o$ (fig. 7(c)); at the same unit Reynolds number for the $\theta_f = 10^o$ model with side plates (fig. 8(c)), the extent of separation increased (to approximately 6.35 cm) and no solution could be found. Attempts to obtain solutions also failed at other unit Reynolds numbers where the extent of separation was greater than that found for the $\theta_f = 10^o$ data. Thus, it appears from these calculations with heat transfer $\left(T_w/T_t = 0.6\right)$ that the Lees and Reeves II method is applicable only for flap angles that will produce a small amount of separation. This same phenomenon appeared to be true from the results of a similar method of calculation by Holden in references 3 and 4.

Laminar Method of Bertram and Feller

(Effect of Pressure Gradient Included)

The capability of predicting laminar heat transfer for hypersonic separated flows by the method of Bertram and Feller (ref. 41) was pointed out by Miller, Hijman, and Childs in reference 7; however, reference 7 shows a limited amount of heat-transfer data and even less application of the Bertram and Feller theory on the flap. The assumption of a constant temperature potential $\left(T_{aw} - T_w\right)$ over the model gives

$$\frac{q}{q_{th,o}} = \frac{\zeta'_w}{(0.664)\left(1 - \zeta_w\right)}\sqrt{2(n+1)\frac{p_e x_o}{p_\infty x}} \tag{20}$$

which is a slight modification of the heat-transfer expression of reference 41. The pressure-gradient parameter n used in equation (20) is related to the pressure by

$$p_e \propto x^n \tag{21}$$

and the similar solution pressure-gradient parameter is related to n by

$$\beta = \left(\frac{1 - \gamma}{\gamma}\right)\frac{n}{n+1} \tag{22}$$

The value of β from equation (22) was used to find the value of ζ'_w from the results of similar solutions shown in figure 14. The similar solutions in figure 14 were made for a

Prandtl number of 1 and a $\rho\mu$ ratio of 1. The Bertram and Feller $q/q_{th,o}$ ratio in figures 7 and 8, calculated from equation (20), used the experimental pressure distribution from references 5 and 6 and the appropriate attached or separated value of ζ'_w from figure 14 as a function of the calculated value of β.

Laminar Separated Flate-Plate Method of Bushnell

The method of Bushnell (ref. 42) considers the reversed flow originating at the reattachment point as analogous to that on a flat plate with the leading edge at the reattachment point and with new edge properties for total enthalpy and velocity based on the separated flow geometry. The method of Bushnell in reference 42 has been modified for application to heat transfer on the present model. The approximate distance normal to the surface from the flap to the dividing streamline is given by

$$\frac{y_*}{L} = \frac{\left[1 - \left(\frac{x}{L}\right)_s\right]\left[\left(\frac{x}{L}\right)_r - \frac{x}{L}\right]\sin\psi}{\left[\left(\frac{x}{L}\right)_r - 1\right]} \tag{23}$$

where ψ is the indicated flow deflection angle over the separated region defined and plotted in reference 5. The maximum reversed-flow velocity is found as a function of the parameter a for separated flow from curves given in reference 42. The value of a is found from

$$a = \frac{0.6456\,\frac{y_*}{L}\,\rho_e u_e\,\frac{T_e}{T_t} - 5.75\times10^6\,\frac{u_e^2}{T_{t,e}} + 1.120}{\sqrt{\int_0^{x/L}\rho_w\mu_w u_e\,d\frac{x}{L}}} \qquad 9.96 - 3.375\times10^5\,\frac{u_e^2}{T_{t,e}} \tag{24}$$

Equation (24) is derived by substituting a curve fit of the integrals of $\int_0^{\eta_*} d\eta$ and $\int_0^{\eta_*} (f')^2 d\eta$ as a function of a and then substituting the two curve fits into

$$\frac{h_{t,e}}{h_e}\left[\int_0^{\eta_*}\zeta\,d\eta - \int_0^{\eta_*}(f')^2 d\eta\left(\frac{u_e^2}{2h_{t,e}}\right)\right] = \frac{u_e\rho_e\left(\frac{y}{L}\right)_*}{\sqrt{2\int_0^{x/L}\rho_w\mu_w u_e\,d\frac{x}{L}}} \tag{25}$$

where f is the stream function (see ref. 36).

The heat-transfer rate on the flap in the region of separated flow is calculated from

$$q = \rho_w \mu_w u_{e,*} \sqrt{\frac{1}{\int_{(x/L)_r}^{x/L} \rho_w \mu_w u_{e,*} \, d\frac{x}{L}}} h_{t,e} \zeta'_w \tag{26}$$

where the value of $u_{e,*}$ is found from the curves of the velocity at the dividing streamline as a function of a.

The value of ζ'_w used in equation (26) was taken from the similar solutions in figure 14 at $\beta = 2.0$ and was held at a constant value of $\zeta'_w = 0.361$ for all calculations. The constant value of ζ'_w used for the afterbody calculations in reference 42, using an equation similar to equation (26), was $\zeta'_w = 0.305$ for $\beta = 0$ condition. The $\beta = 0$ condition used in reference 42 was applicable for the essentially constant pressure over the afterbody separated region; however, for application to the separated reversed flow over the flap, the pressure gradient in the upstream direction is extremely favorable for all cases and a value of $\beta = 2.0$ was considered to apply to all calculations over the flap.

The value of enthalpy used in the equation of reference 42 similar to equation (26) of the present report was approximately half of the free-stream total enthalpy. In the present report, the entire value of the free-stream total enthalpy was used, and the agreement with the data was better than when a fraction of the total enthalpy was used. It is believed that the use of the free-stream total enthalpy gives better results for the flap type of separation because the dividing streamline reattaches on the flap and the rearward stagnation point is on the flap. However, for afterbody separation flow which has a dividing streamline that never reattaches on the model and has a rearward stagnation point which is not on the surface of the model a value of heat-transfer potential that is some fraction of the total enthalpy could be used.

REFERENCES

1. Harvey, William D.: Experimental Investigation of Laminar-Flow Separation on a Flat Plate Induced by Deflected Trailing-Edge Flap at Mach 19. NASA TN D-4671, 1968.

2. Holden, Michael: Separated Flow Studies at Hypersonic Speeds – Part II. Two-Dimensional Wedge Separated Flow Studies. Rep. No. AF-1285-A-13(2) (Contract No. Nonr 2653(00)), Cornell Aeron. Lab., Inc., Dec. 1964.

3. Holden, Michael S.: Leading-Edge Bluntness and Boundary-Layer Displacement Effects on Attached and Separated Laminar Boundary Layers in a Compression Corner. AIAA Pap. No. 68-68, Jan. 1968.

4. Holden, M. S.: An Analytical Study of Separated Flows Induced by Shock Wave – Boundary Layer Interaction. Rep. No. A1-1972-A-3 (Contract NAS 5-3976), Cornell Aeron. Lab., Inc., Dec. 1965.

5. Johnson, Charles B.: Pressure and Flow-Field Study at Mach Number 8 of Flow Separation on a Flat Plate With Deflected Trailing-Edge Flap. NASA TN D-4308, 1968.

6. Johnson, Charles Borden: A Theoretical and Experimental Study at Mach 8 of Flow Separation of a Flat Plate With Deflected Trailing Edge Flap. M.S. Thesis, Virginia Polytech. Inst., 1966.

7. Miller, D. S.; Hijman, R.; and Childs, M. E.: Mach 8 to 22 Studies of Flow Separations Due to Deflected Control Surfaces. AIAA J., vol. 2, no. 2, Feb. 1964, pp. 312-321.

8. Burchfield, C. G.; Hube, F. K.; and Burdette, J. E.: An Experimental Heat-Transfer Investigation in Regions of Flow Separation at Mach Number 8. AEDC-TDR-64-30, U.S. Air Force, Feb. 1964.

9. Kaufman, Louis G., II: Pressure and Heat Transfer Measurements for Hypersonic Flows Over Expansion Corners and Ahead of Ramps – Part IV: Mach 8 Heat Transfer Data for Flows Ahead of Ramps. ASD-TDR-63-679, Pt. IV, U.S. Air Force, July 1964. (Available from DDC as AD 607 038.)

10. Kaufman, L. G., II; Meckler, L.; and Hartofilis, S. A.: An Investigation of Flow Separation and Aerodynamic Controls at Hypersonic Speeds. J. Aircraft, vol. 3, no. 6, Nov.-Dec. 1966, pp. 555-561.

11. Gulbran, C. E.; Redeker, E.; Miller, D. S.; and Strack, S. L.: Heating in Regions of Interfering Flow Fields – Part I. Two- and Three-Dimensional Laminar Interactions at Mach 8. AFFDL-TR-65-49, Pt. I, U.S. Air Force, July 23, 1965.

12. Kaufman, Louis G., II; Meckler, Lawrence H.; Hartofilis, Stavros A.; and Weiss, Daniel: An Investigation of Hypersonic Flow Separation and Control Characteristics. AFFDL-TR-64-174, U.S. Air Force, Jan. 1965.

13. Popinski, Z.: Shock Wave-Boundary Layer Interaction. Proceedings of the Third International Heat Transfer Conference – Vol. II, Amer. Inst. Chem. Eng., Aug. 7-12, 1966, pp. 262-273.

14. Giles, H. L.; and Thomas, J. W.: Analysis of Hypersonic Pressure and Heat Transfer Tests on a Flat Plate With a Flap and a Delta Wing With Body, Elevons, Fins, and Rudders. NASA CR-536, 1966.

15. Holloway, Paul F.; Sterrett, James R.; and Creekmore, Helen S.: An Investigation of Heat Transfer Within Regions of Separated Flow at a Mach Number of 6.0. NASA TN D-3074, 1965.

16. Chapman, Dean R.; Kuehn, Donald M.; and Larson, Howard K.: Investigation of Separated Flows in Supersonic and Subsonic Streams With Emphasis on the Effect of Transition. NACA Rep. 1356, 1958. (Supersedes NACA TN 3869.)

17. Schaefer, John W.; and Ferguson, Harold: Investigation of Separation and the Associated Heat Transfer and Pressure Distribution on Cone-Cylinder-Flare Configurations at Mach Five. ARS J., vol. 32, no. 5, May 1962, pp. 762-769.

18. Sterrett, J. R.; and Holloway, P. F.: On the Effect of Transition on Parameters Within a Separation Region at Hypersonic Speeds – With Emphasis on Heat Transfer. Symposium on Fully Separated Flows, Authur G. Hansen, ed., Amer. Soc. Mech. Eng., May 1964, pp. 15-26.

19. Whitehead, Allen H., Jr.; and Keyes, J. Wayne: Flow Phenomena and Separation Over Delta Wings With Trailing-Edge Flaps at Mach 6. AIAA J., vol. 6, no. 12, Dec. 1968, pp. 2380-2387.

20. Needham, D. A.; and Stollery, J. L.: Hypersonic Studies of Incipient Separation and Separated Flows. Separated Flows, Pt. I, AGARD CP No. 4, May 1966, pp. 89-119.

21. Becker, John V.; and Korycinski, Peter F.: Heat Transfer and Pressure Distribution at a Mach Number of 6.8 on Bodies With Conical Flares and Extensive Flow Separation. NASA TN D-1260, 1962.

22. Bogdonoff, S. M.; and Vas, I. E.: Some Experiments on Hypersonic Separated Flows. ARS J., vol. 32, no. 10, Oct. 1962, pp. 1564-1572.

23. Hartofilis, Stavros A.: Pressure and Heat Transfer Measurements at Mach 13 and 19 for Flows Ahead of Ramps, Over Expansion Corners, and Past Fin-Plate Combinations. Rep. No. FDL-TDR-64-144, U.S. Air Force, Sept. 1964. (Available from DDC as AD 608 048.)

24. Hamilton, H. Harris; and Dearing, J. David: Effect of Hinge-Line Bleed on Heat Transfer and Pressure Distribution Over a Wedge-Flap Combination at Mach 10.4. NASA TN D-4686, 1968.

25. Needham, David A.: A Heat-Transfer Criterion for the Detection of Incipient Separation in Hypersonic Flow. AIAA J. (Tech. Notes), vol. 3, no. 4, Apr. 1965, pp. 781-783.

26. Chilcott, R. E.: A Review of Separated and Reattaching Flows With Heat Transfer. Int. J. Heat Mass Transfer, vol. 10, no. 6, June 1967, pp. 783-797.

27. Wuerer, J. E.; and Clayton, F. I.: Flow Separation in High Speed Flight – A Review of the State-of-the-Art. Rep. SM-46429, Missile & Space Syst. Div., Douglas Aircraft Co., Apr. 1965.

28. Kaufman, Louis G., II; Hartofilis, Stavros A.; Evans, William J.; Oman, Richard A.; Meckler, Lawrence H.; and Weiss, Daniel: A Review of Hypersonic Flow Separation and Control Characteristics. ASD-TDR-62-168, U.S. Air Force, Mar. 1962.

29. Neilsen, Jack N.; and Goodwin, Frederick K.: Investigation of Hypersonic Flow Separation and Its Effect on Aerodynamic Control Characteristics. Vidya Rep. No. 63 (Contract No. AF 33(657)-7084), Itek Corp., Jan. 1962.

30. Clayton, F. I.; and Wuerer, J. E.: Flow Separation in High-Speed Flight. A Report Bibliography. DAC-59101, Missile & Space Syst. Div., Douglas Aircraft Co., Inc., Sept. 1966.

31. Stainback, P. Calvin: Heat-Transfer Measurements at a Mach Number of 8 in the Vicinity of a 90° Interior Corner Alined With the Free-Stream Velocity. NASA TN D-2417, 1964.

32. Schaefer, William T., Jr.: Characteristics of Major Active Wind Tunnels at the Langley Research Center. NASA TM X-1130, 1965.

33. Stainback, P. Calvin: Heat-Transfer Measurements at a Mach Number of 4.95 on Two 60° Swept Delta Wings With Blunt Leading Edges and Dihedral Angles of 0° and 45°. NASA TN D-549, 1961.

34. Ginoux, Jean J.: Supersonic Separated Flows Over Wedges and Flares With Emphasis on a Method of Detecting Transition. ARL 69-0009, U.S. Air Force, Jan. 1969.

35. Schlichting, Hermann (J. Kestin, trans.): Boundary Layer Theory. Fourth ed., McGraw-Hill Book Co., Inc., c.1960, p. 389.

36. Beckwith, Ivan E.; and Cohen, Nathaniel B.: Application of Similar Solutions to Calculation of Laminar Heat Transfer on Bodies With Yaw and Large Pressure Gradient in High-Speed Flow. NASA TN D-625, 1961.

37. Monaghan, R. J.: On the Behavior of Boundary Layers at Supersonic Speeds. Fifth International Aeronautical Conference, Rita J. Turino and Caroline Taylor, eds., Inst. Aeron. Sci., Inc., June 1955, pp. 277-315.

38. Van Driest, E. R.: The Problem of Aerodynamic Heating. Aeronaut. Eng. Rev., vol. 15, no. 10, Oct. 1956, pp. 26-41.

39. Chapman, Dean R.: A Theoretical Analysis of Heat Transfer in Regions of Separated Flow. NACA TN 3792, 1956.

40. Lees, Lester; and Reeves, Barry L.: Supersonic Separated and Reattaching Laminar Flows: I. General Theory and Application to Adiabatic Boundary-Layer Shock-Wave Interactions. AIAA J., vol. 2, no. 11, Nov. 1964, pp. 1907-1920.

41. Bertram, Mitchel H.; and Feller, William V.: A Simple Method for Determining Heat Transfer, Skin Friction, and Boundary-Layer Thickness for Hypersonic Laminar Boundary-Layer Flows in a Pressure Gradient. NASA MEMO 5-24-59L, 1959.

42. Bushnell, Dennis M.: Local Afterbody Heat Transfer to a Blunt Two-Dimensional Configuration at Mach 8. NASA TN D-4443, 1968.

43. Peterson, John B., Jr.: A Comparison of Experimental and Theoretical Results for the Compressible Turbulent-Boundary-Layer Skin Friction With Zero Pressure Gradient. NASA TN D-1795, 1963.

44. Van Driest, E. R.: Turbulent Boundary Layer in Compressible Fluids. J. Aeronaut. Sci., vol. 18, no. 3, Mar. 1951, pp. 145-160, 216.

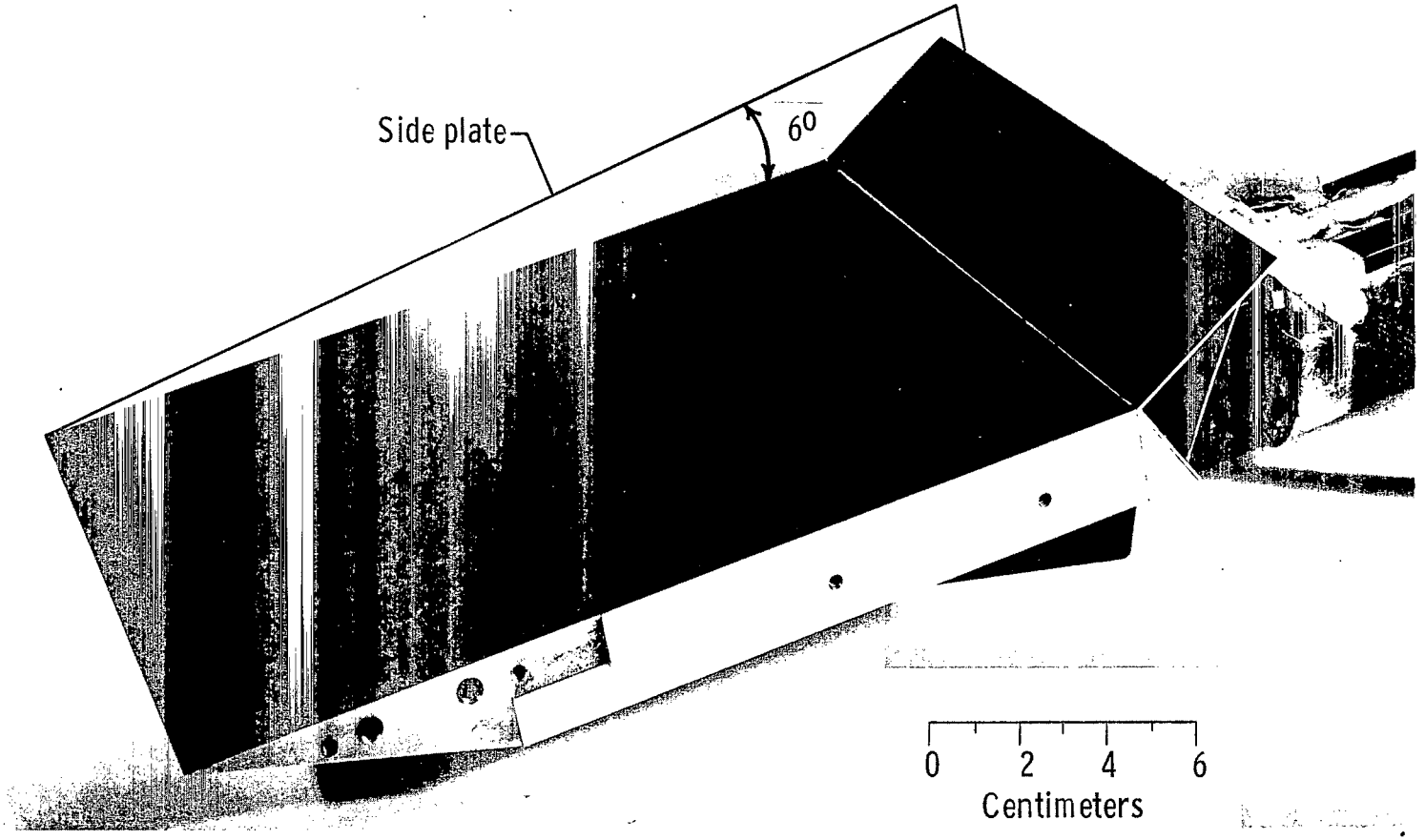

Figure 1.- Photograph of heat-transfer model.

L-65-7665

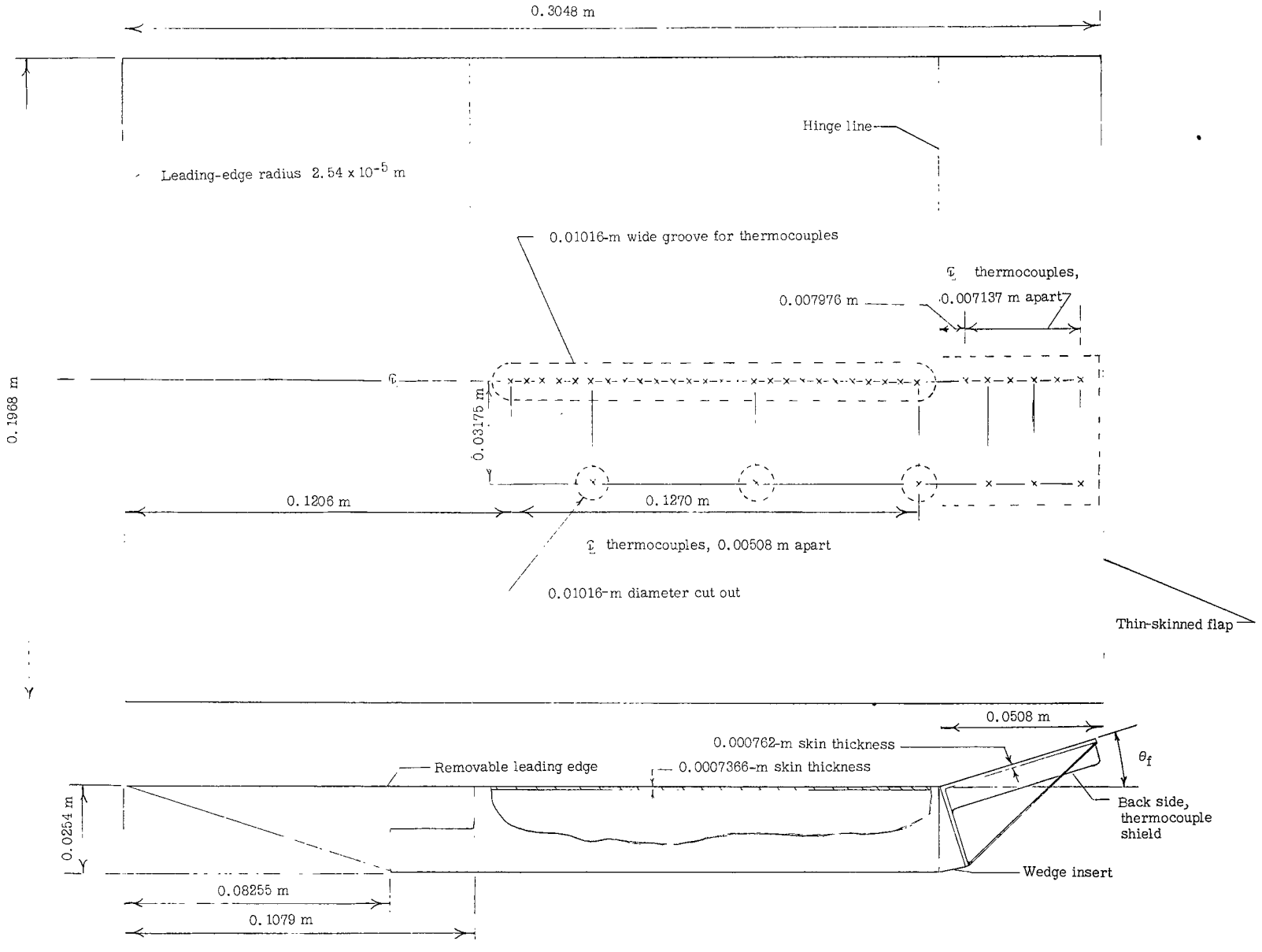

Figure 2.- Schematic of the heat-transfer model. All dimensions are in meters.

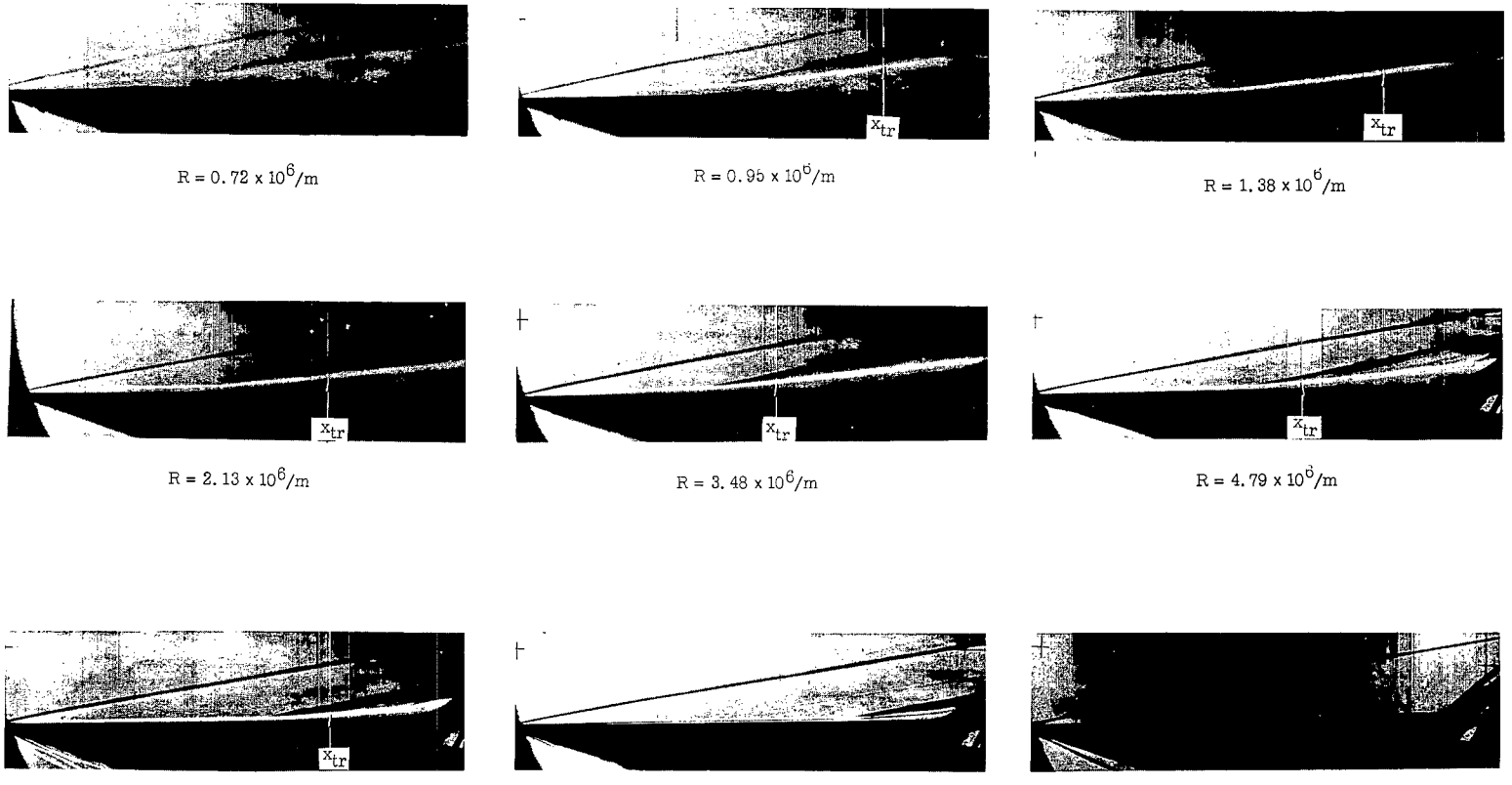

(a) $\theta_f = 30^0$.

L-70-1624

Figure 3.- Schlieren photographs of the flow-separation model at $T_w/T_t \approx 0.4$ for three flap angles and various unit Reynolds numbers.

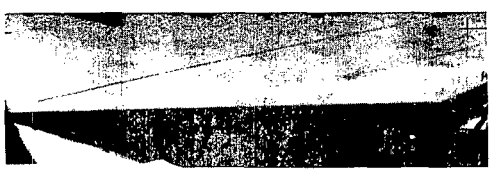

$R = 0.72 \times 10^6/m$

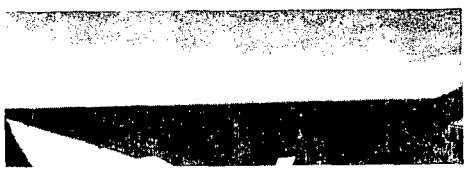

$R = 0.95 \times 10^6/m$

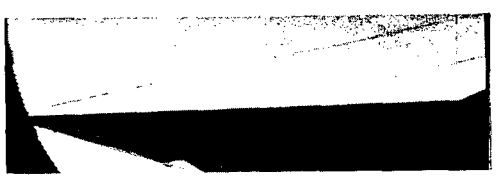

$R = 1.38 \times 10^6/m$

$R = 2.13 \times 10^6/m$

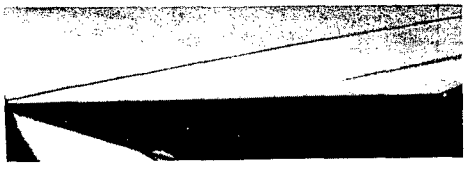

$R = 3.48 \times 10^6/m$

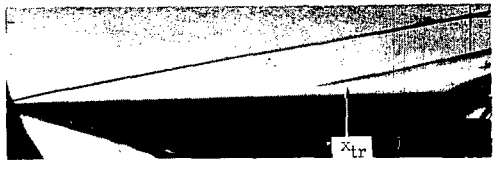

$R = 4.79 \times 10^6/m$

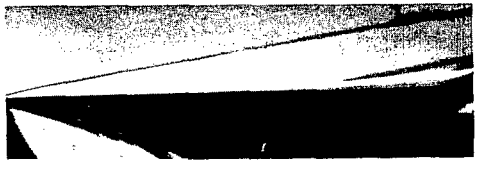

$R = 8.69 \times 10^6/m$

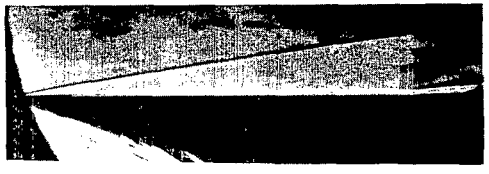

$R = 14.10 \times 10^6/m$

(b) $\theta_f = 20^o$.

L-70-1625

Figure 3.- Continued.

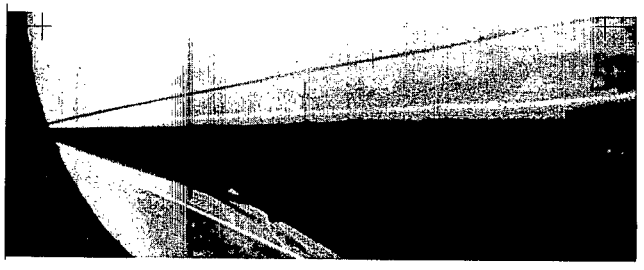

$R = 2.13 \times 10^6/m$

$R = 1.38 \times 10^6/m$

$R = 3.48 \times 10^6/m$

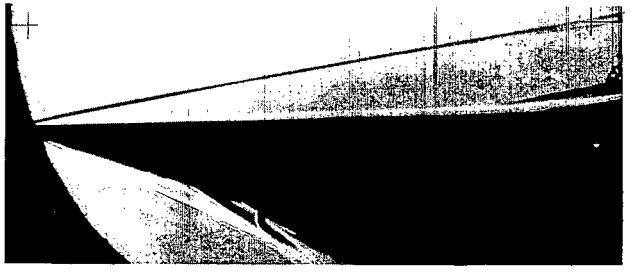

$R = 4.79 \times 10^6/m$

(c) $\theta_f = 10^o$.

L-70-1626

Figure 3.- Concluded.

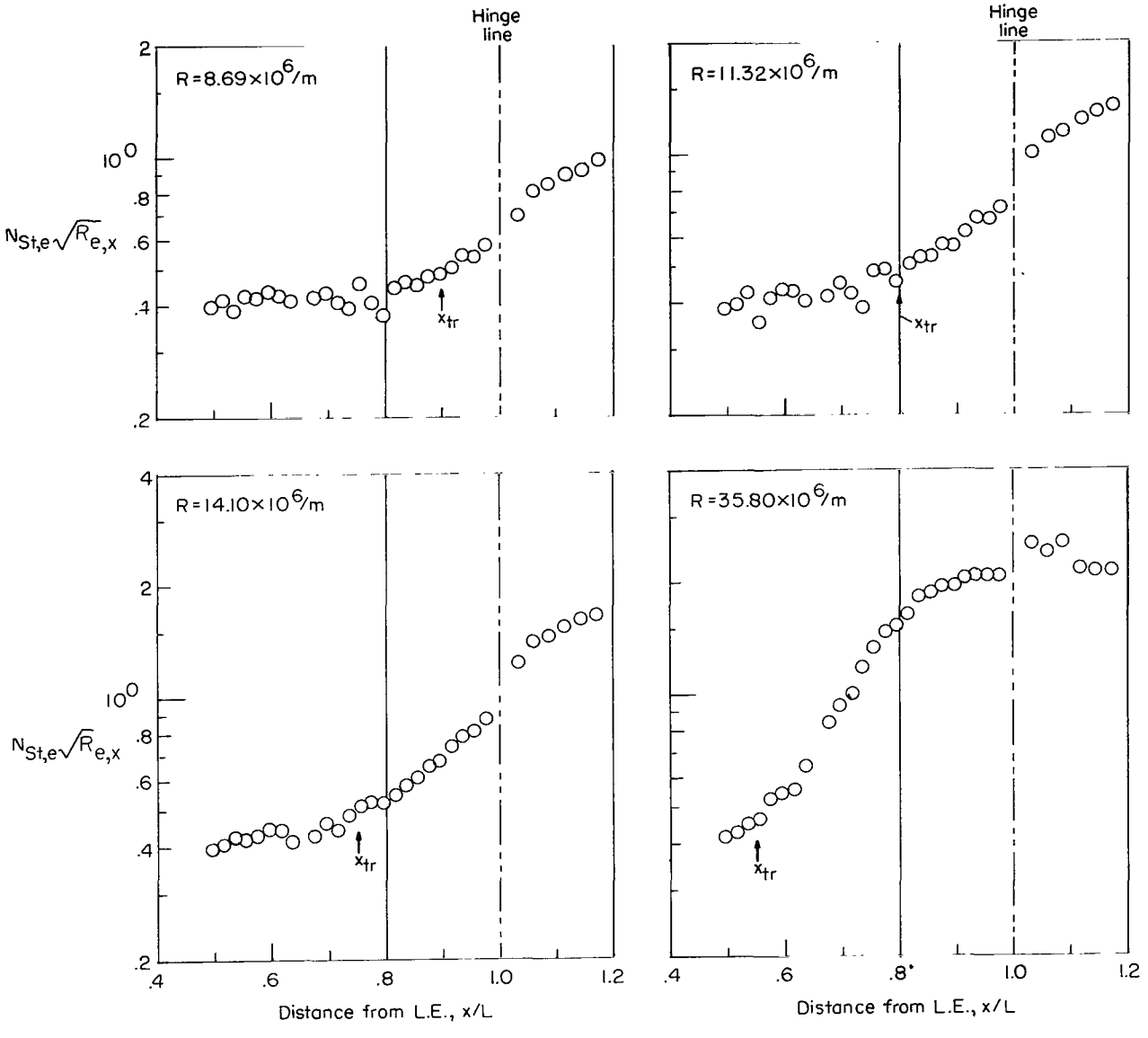

Figure 4.- The effect of Reynolds number on the location of the start of transition for $\theta_f = 0^0$ at $T_w/T_t \approx 0.4$ for the model without side plates.

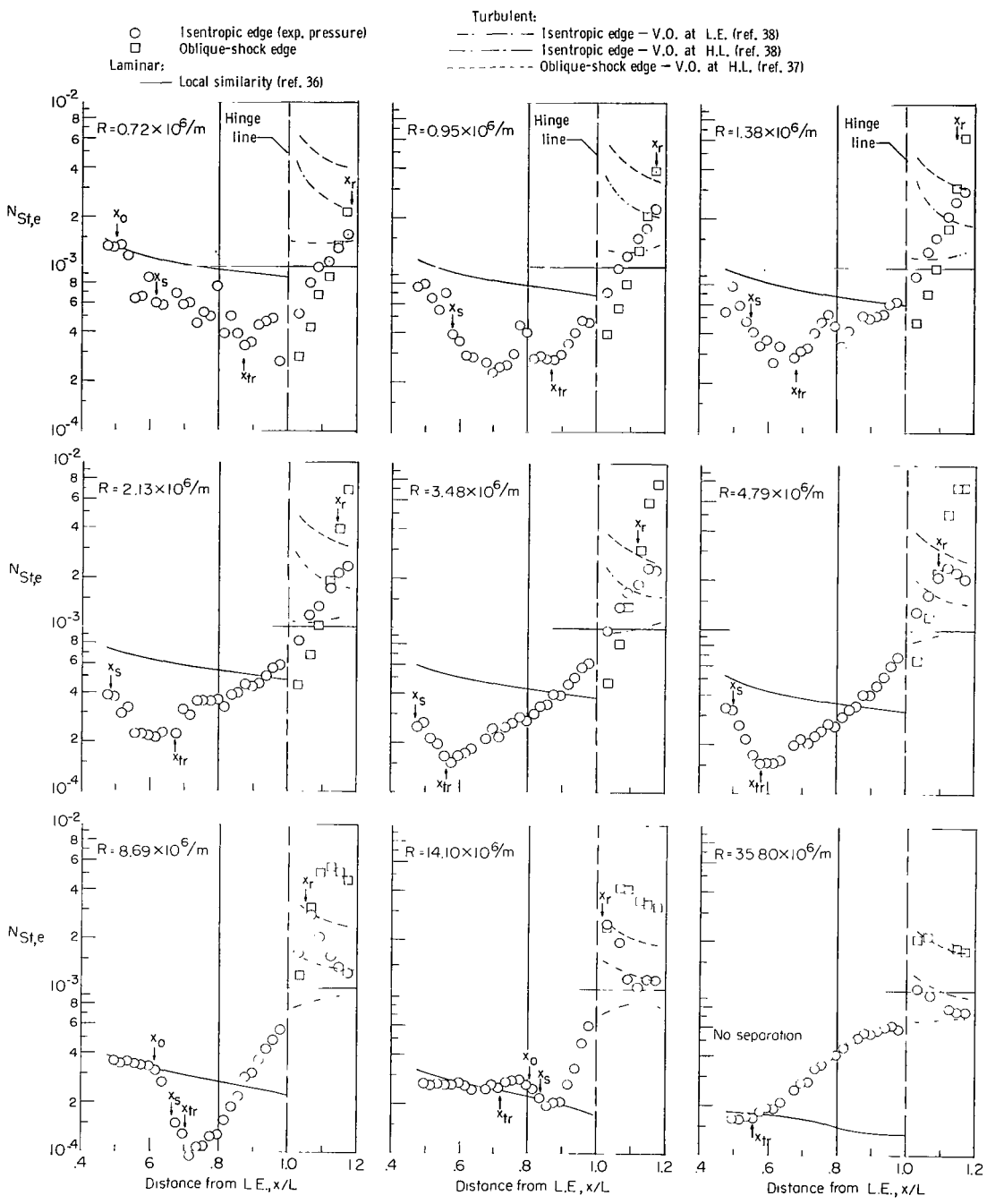

(a) $\theta_f = 30^0$.

Figure 5.- The effect of Reynolds number on heat transfer in terms of Stanton number at $T_W/T_t \approx 0.4$ for three flap angles. (Abbreviations: V.O. is vertual origin; L.E. is leading edge; H.L. is hinge line; and exp. is experimental.)

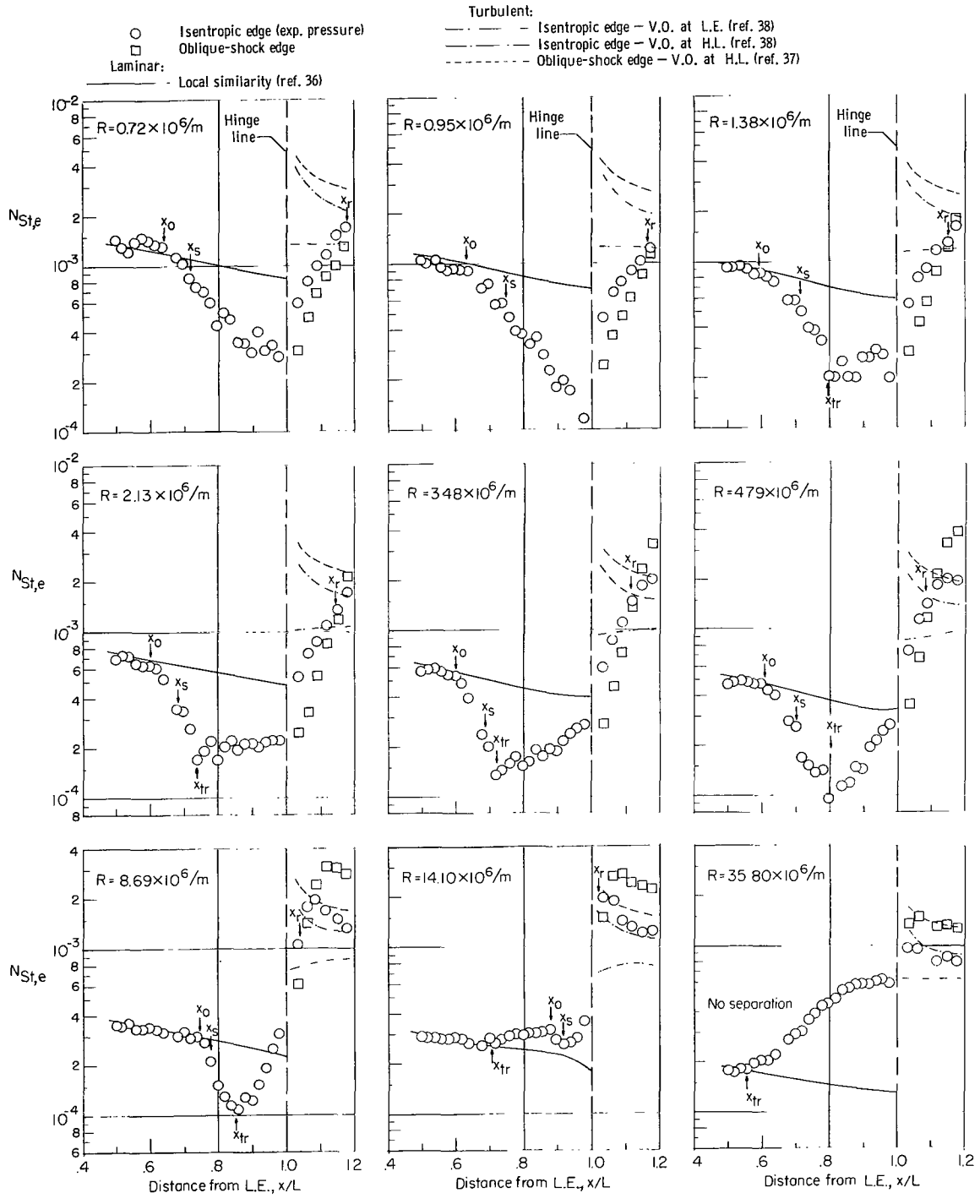

(b) $\theta_f = 20^0$.

Figure 5.- Continued.

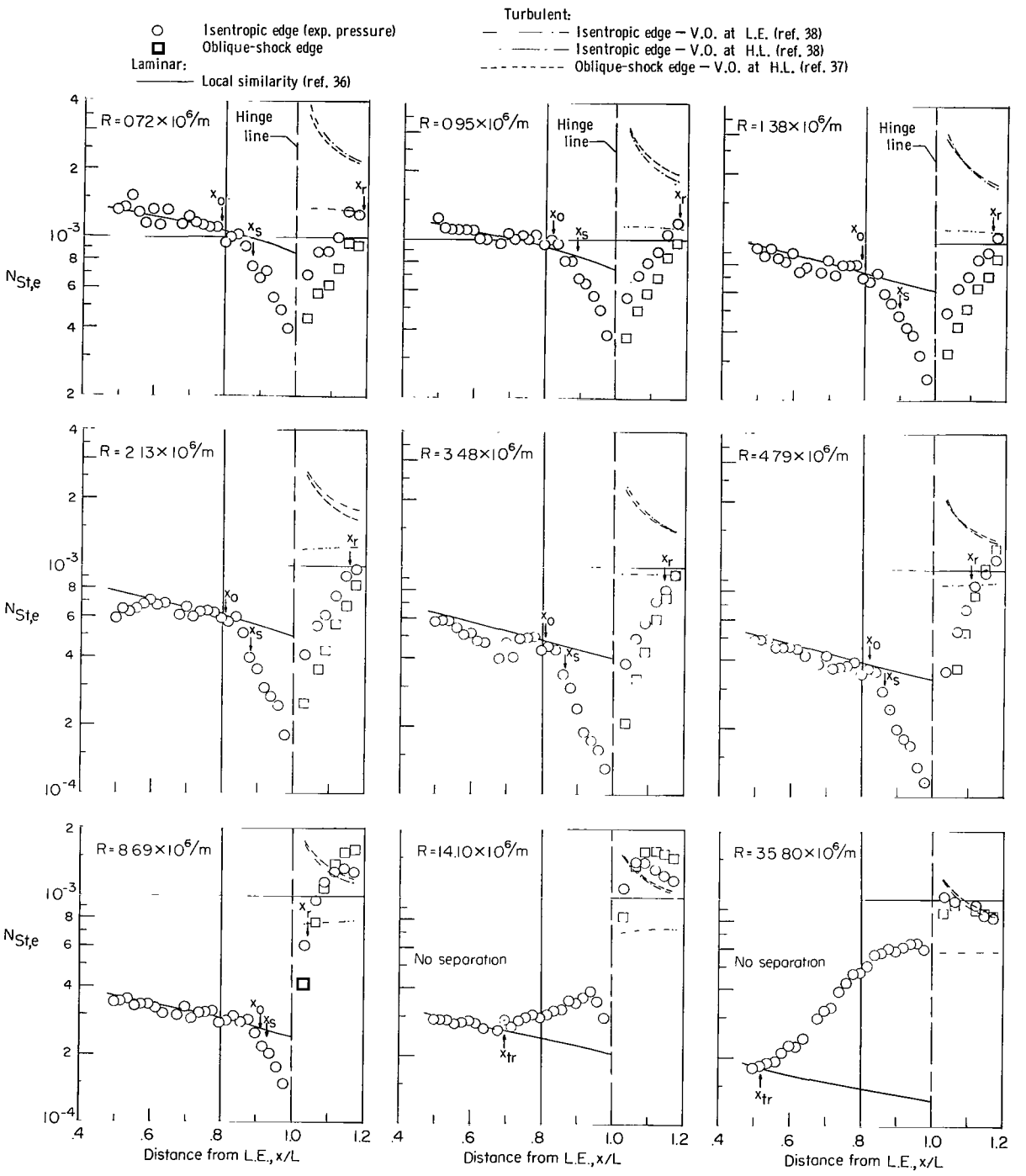

(c) $\theta_f = 10^0$.

Figure 5.- Concluded.

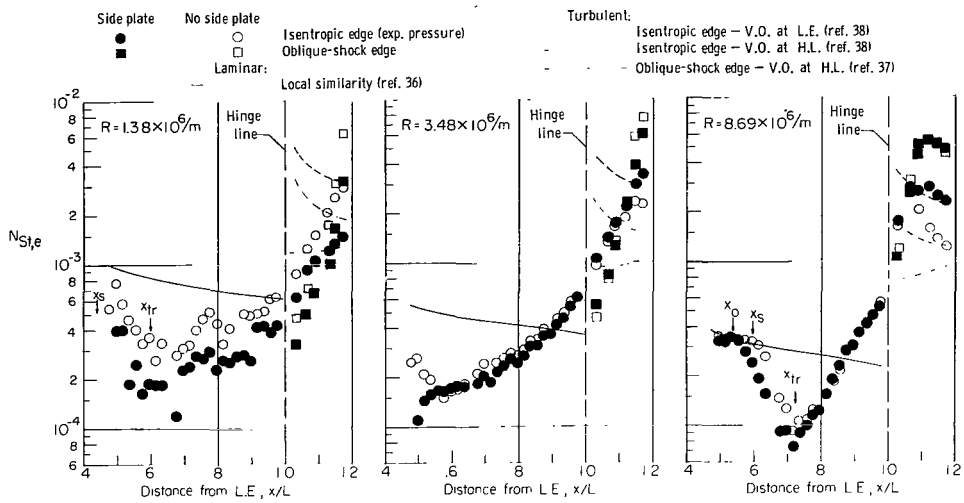

(a) $\theta_f = 30^0$.

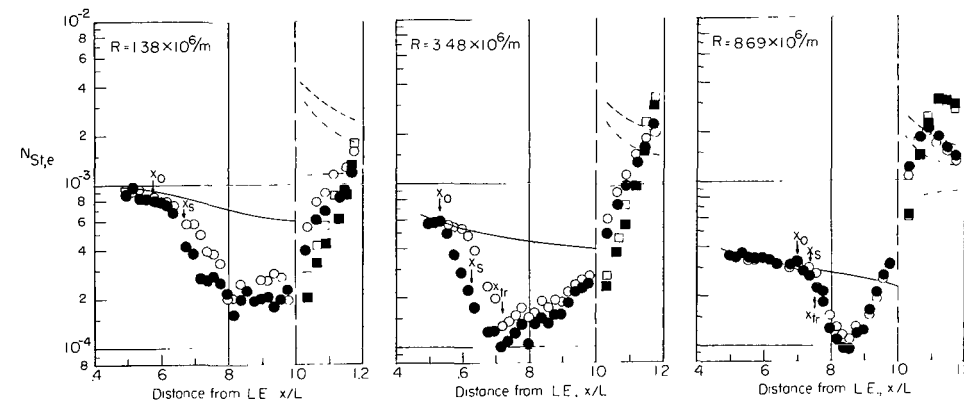

(b) $\theta_f = 20^0$.

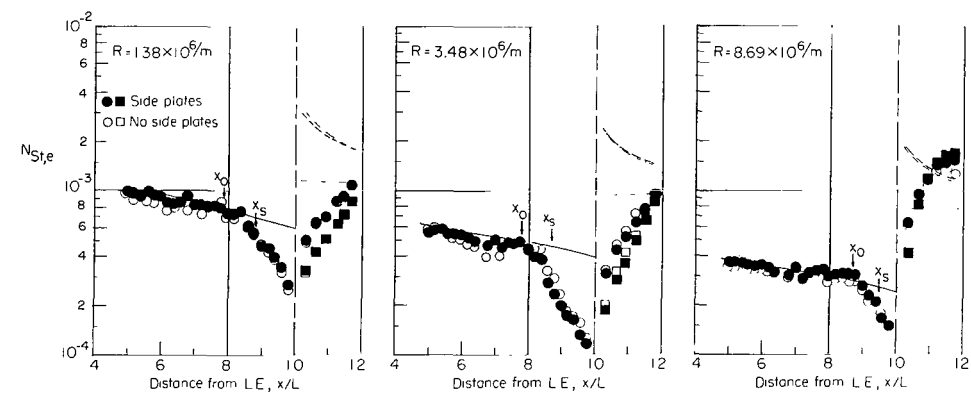

(c) $\theta_f = 10^0$.

Figure 6.- The effect of side plates on the variation of Reynolds number with heat transfer in terms of Stanton number at $T_w/T_t \approx 0.4$ for three flap angles. The locations x_s, x_{tr}, and x_o are for the model with side plates. (Abbreviations: V.O. is virtual origin; L.E. is leading edge; H.L. is hinge line; and exp. is experimental.)

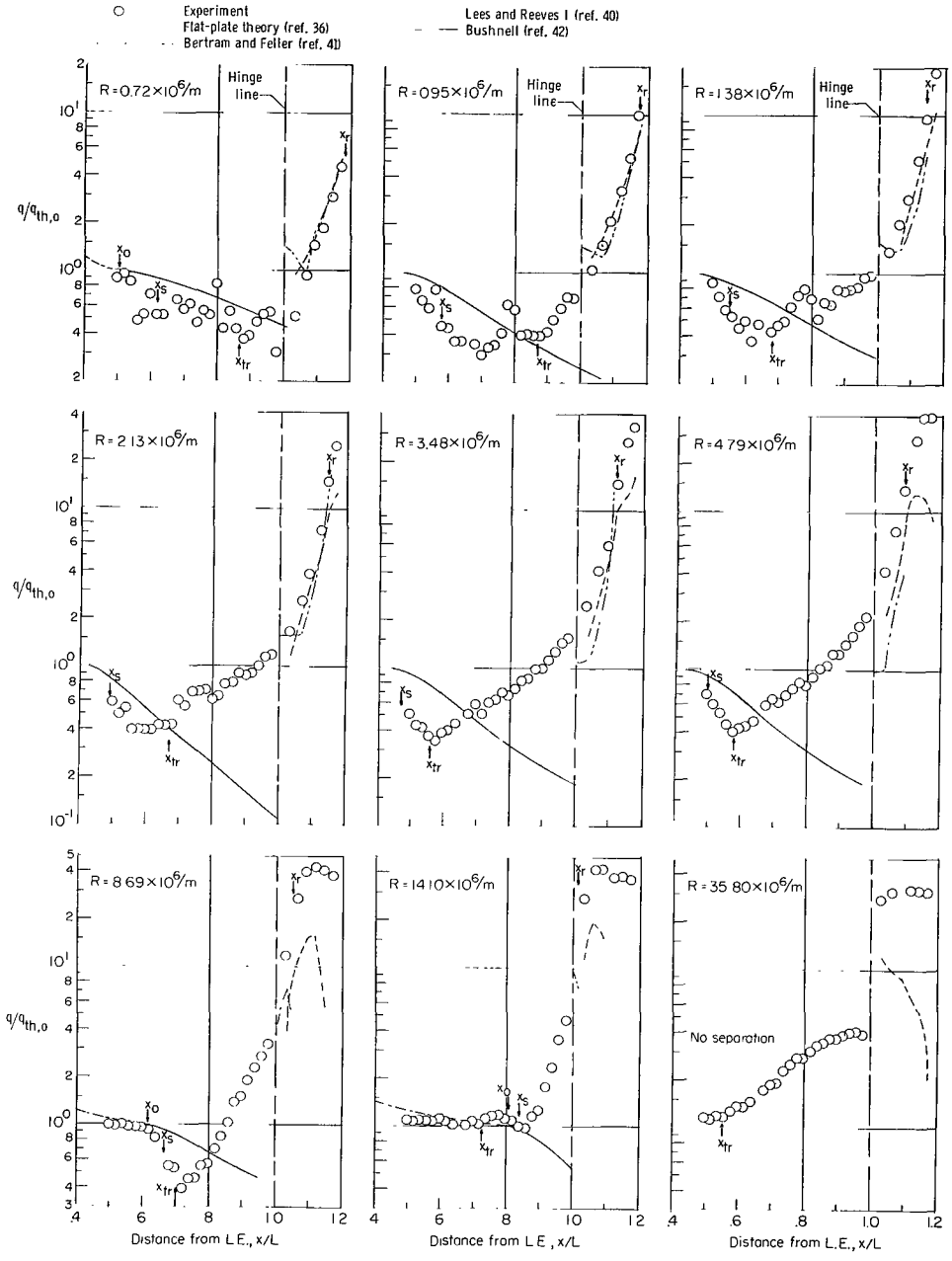

(a) $\theta_f = 30^0$.

Figure 7.- The effect of Reynolds number on heat transfer in terms of heating-rate ratio at $T_W/T_t \approx 0.4$ for three flap angles for the model without side plates. All theoretical predictions were obtained from laminar theory.

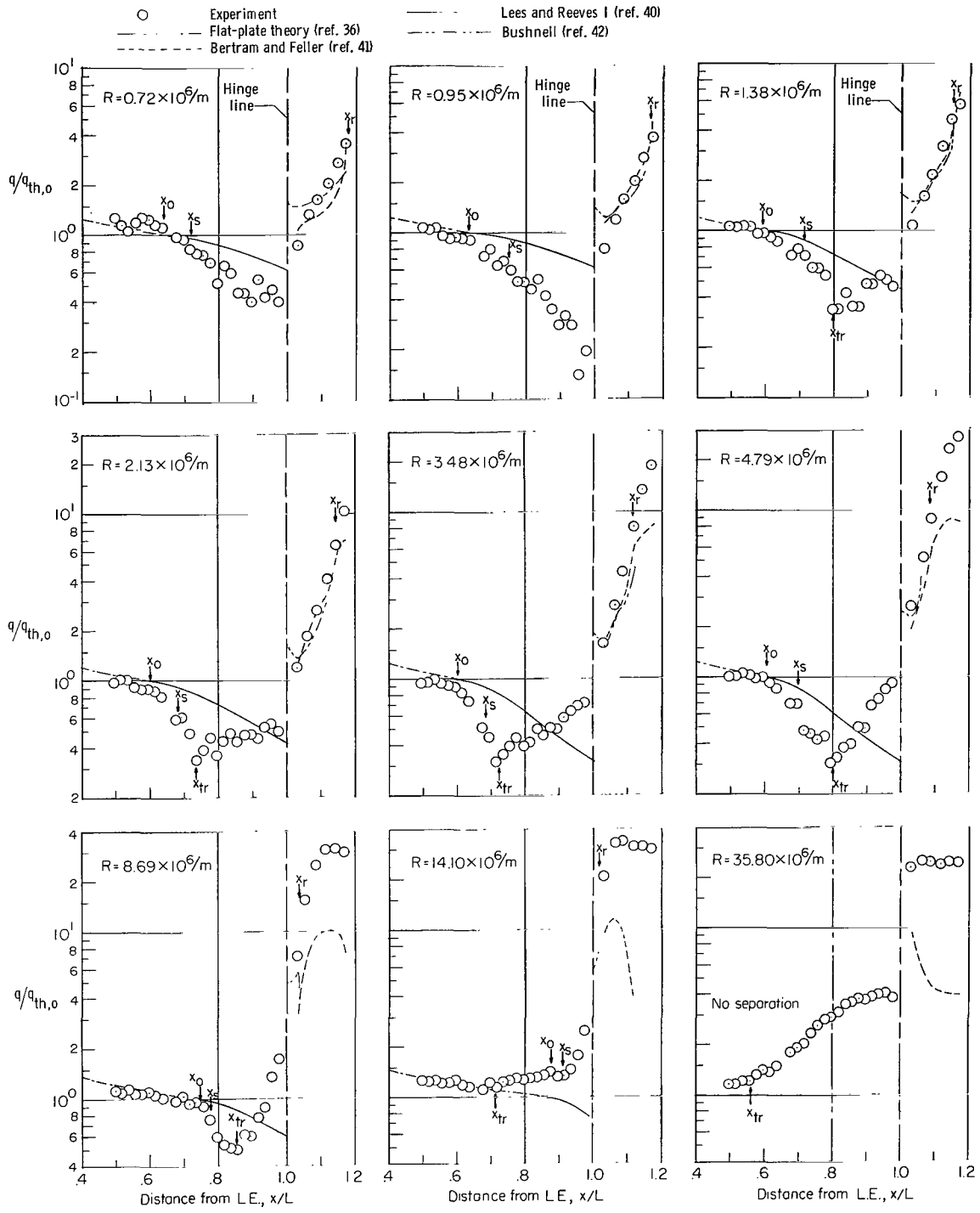

(b) $\theta_f = 20^0$.

Figure 7.- Continued.

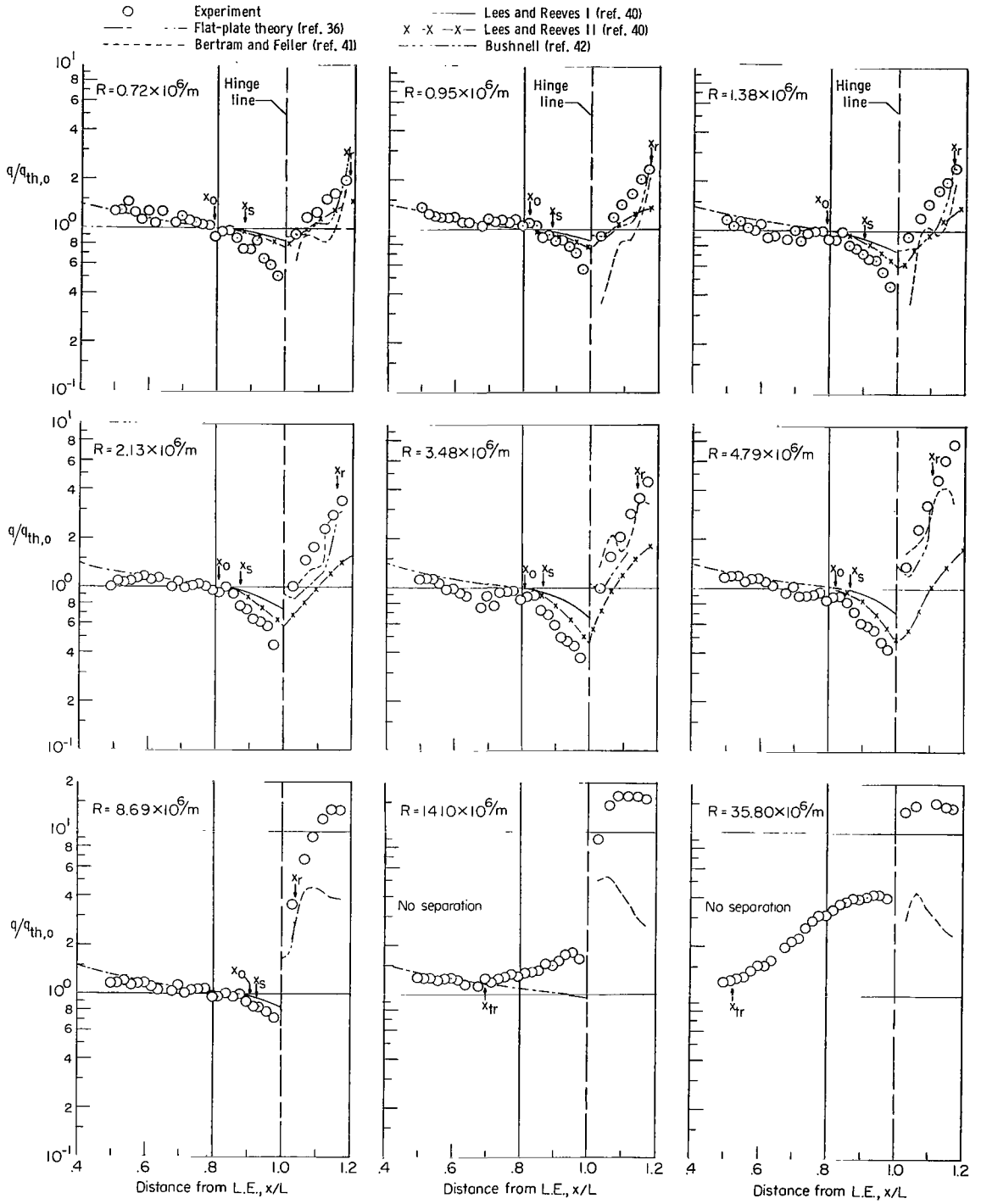

(c) $\theta_f = 10^0$.

Figure 7.- Concluded.

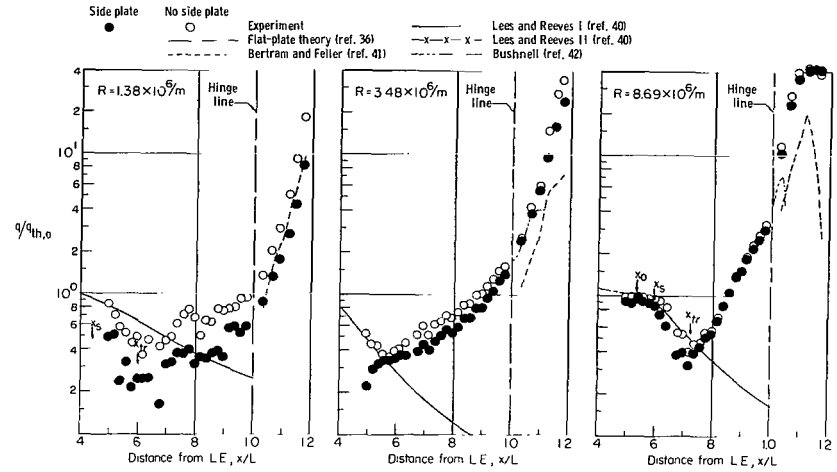

(a) $\theta_f = 30^0$.

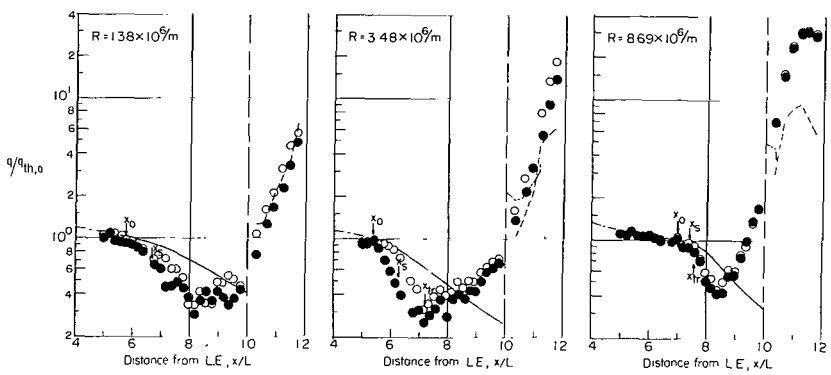

(b) $\theta_f = 20^0$.

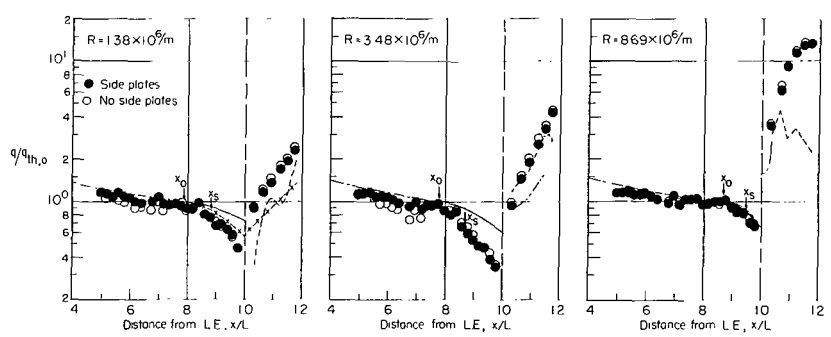

(c) $\theta_f = 10^0$.

Figure 8.- The effect of side plates on the variation of Reynolds number with heat transfer in terms of heating-rate ratio at $T_W/T_t \approx 0.4$ for three flap angles. The locations x_s, x_{tr}, and x_0 are for the model with side plates.

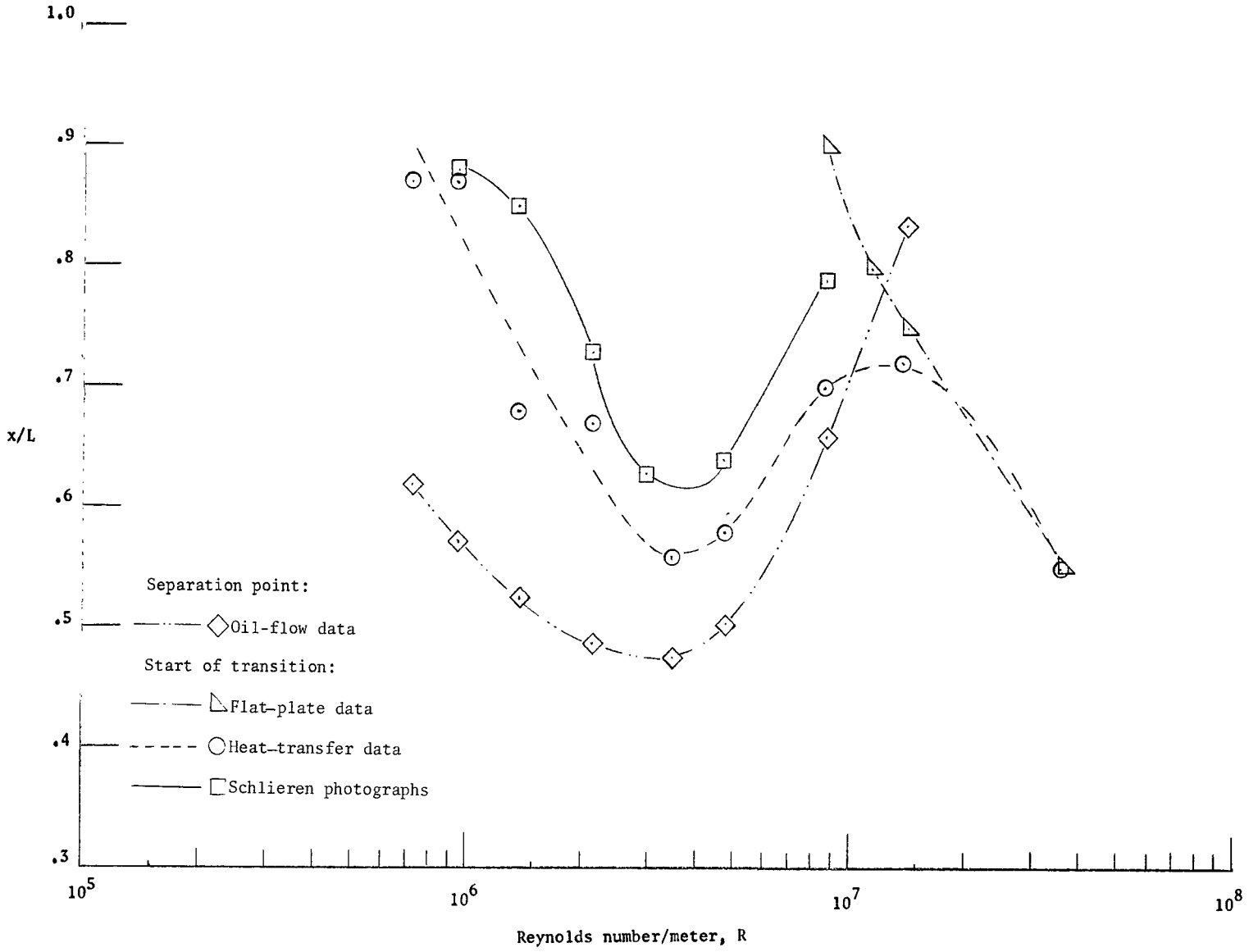

(a) $\theta_f = 30^0$.

Figure 9.- The effect of Reynolds number on location of transition point and separation point.

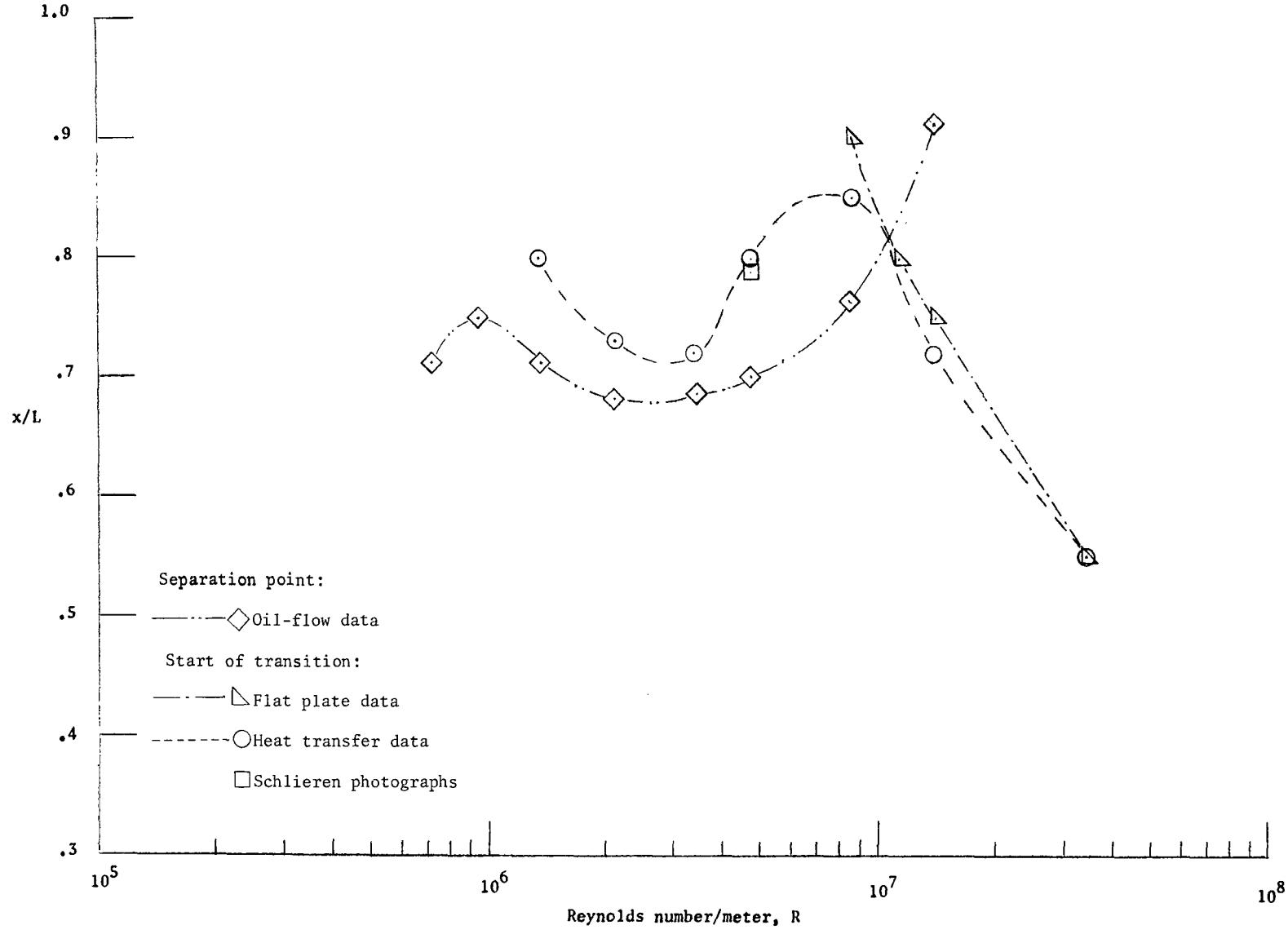

(b) $\theta_f = 20^0$.

Figure 9.- Concluded.

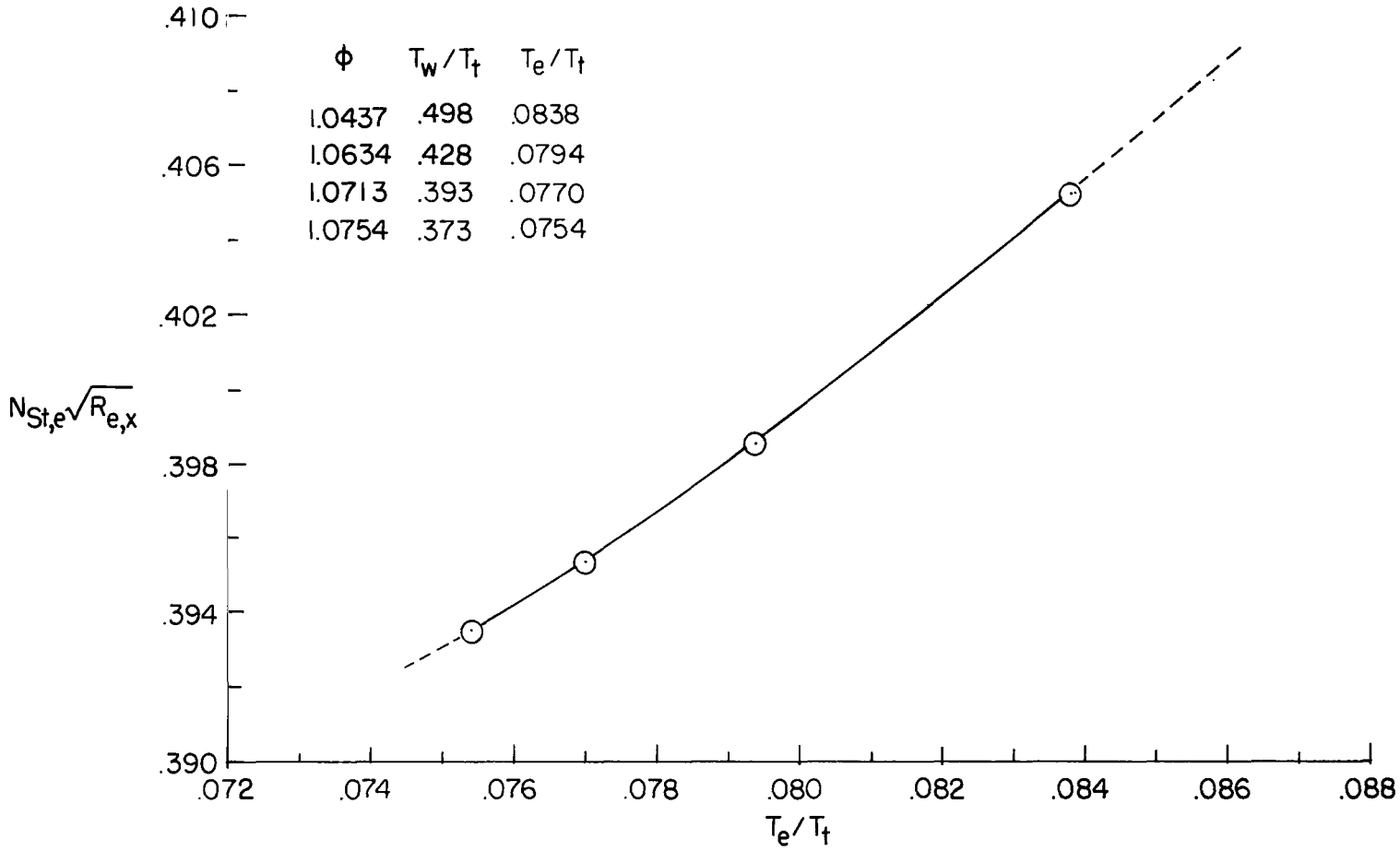

Figure 10.- The variation of laminar flat-plate ($\beta = 0$) heat-transfer parameter from similar solutions over the range of experimental free-stream-to-total temperature ratio. $N_{Pr} = 0.72$.

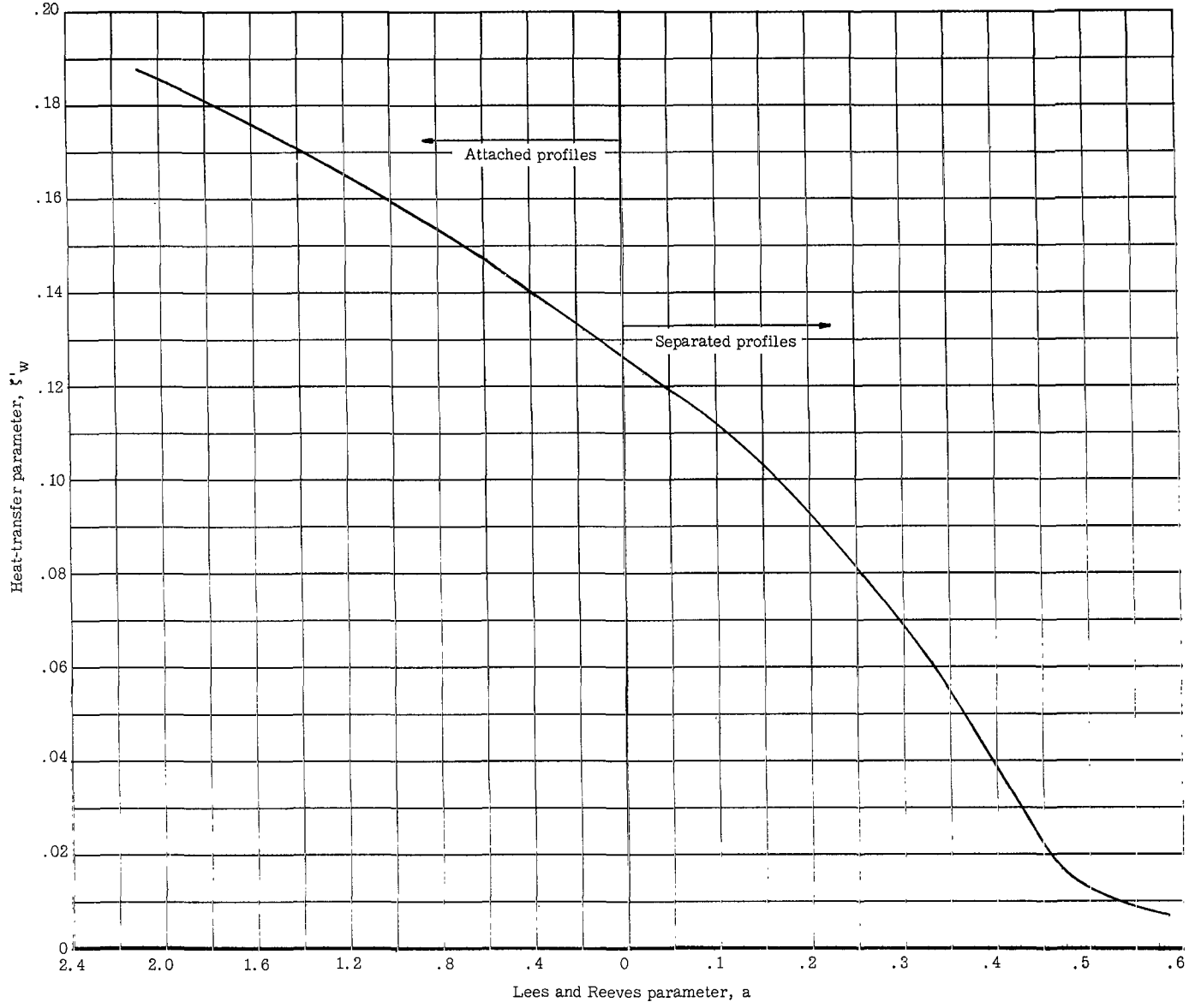

Figure 11.- The heat-transfer parameter from similar solutions as a function of the Lees and Reeves parameter. $T_w/T_t = 0.6$.

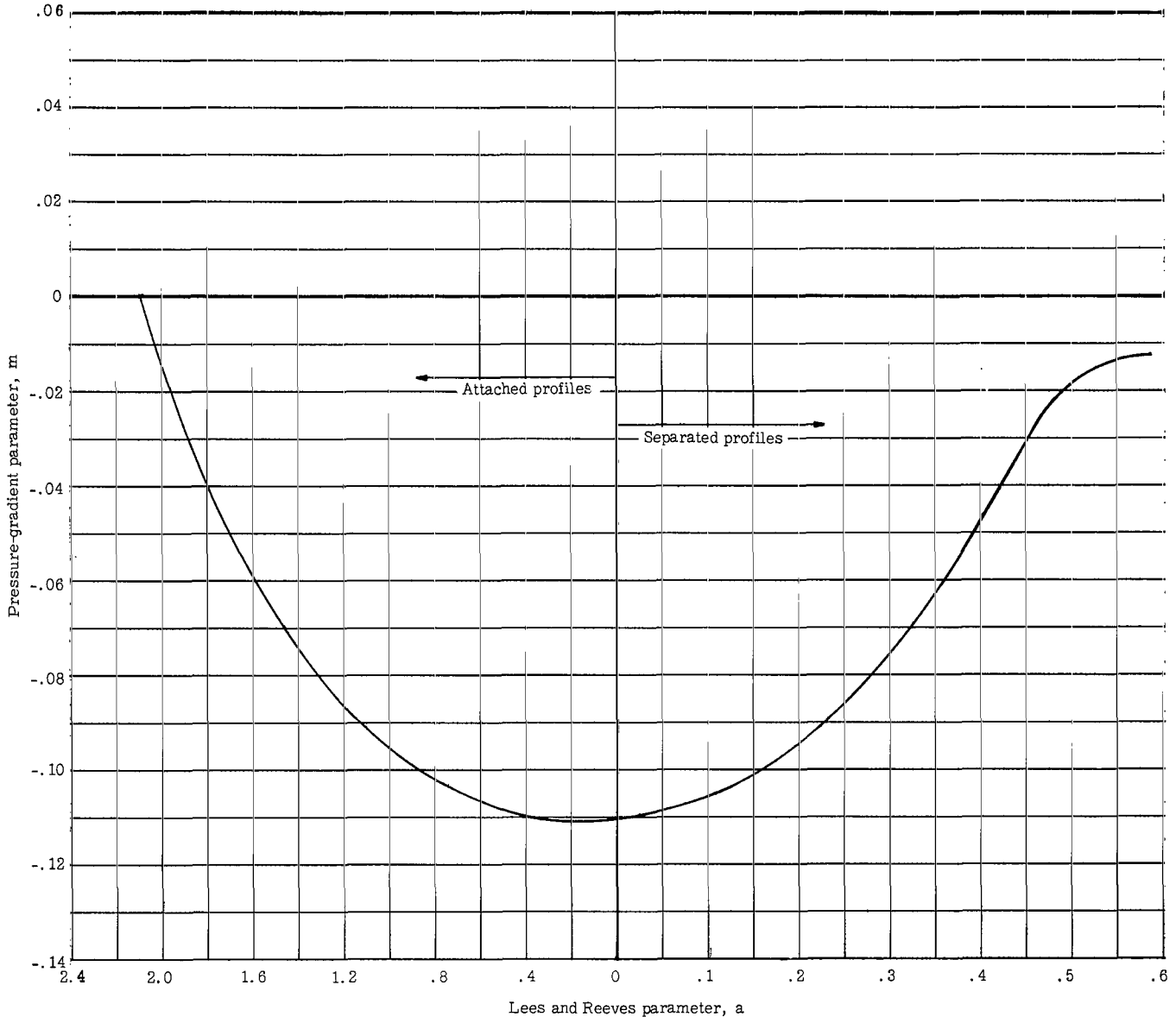

Figure 12.- The pressure-gradient parameter from similar solutions as a function of the Lees and Reeves parameter. $T_w/T_t = 0.6$.

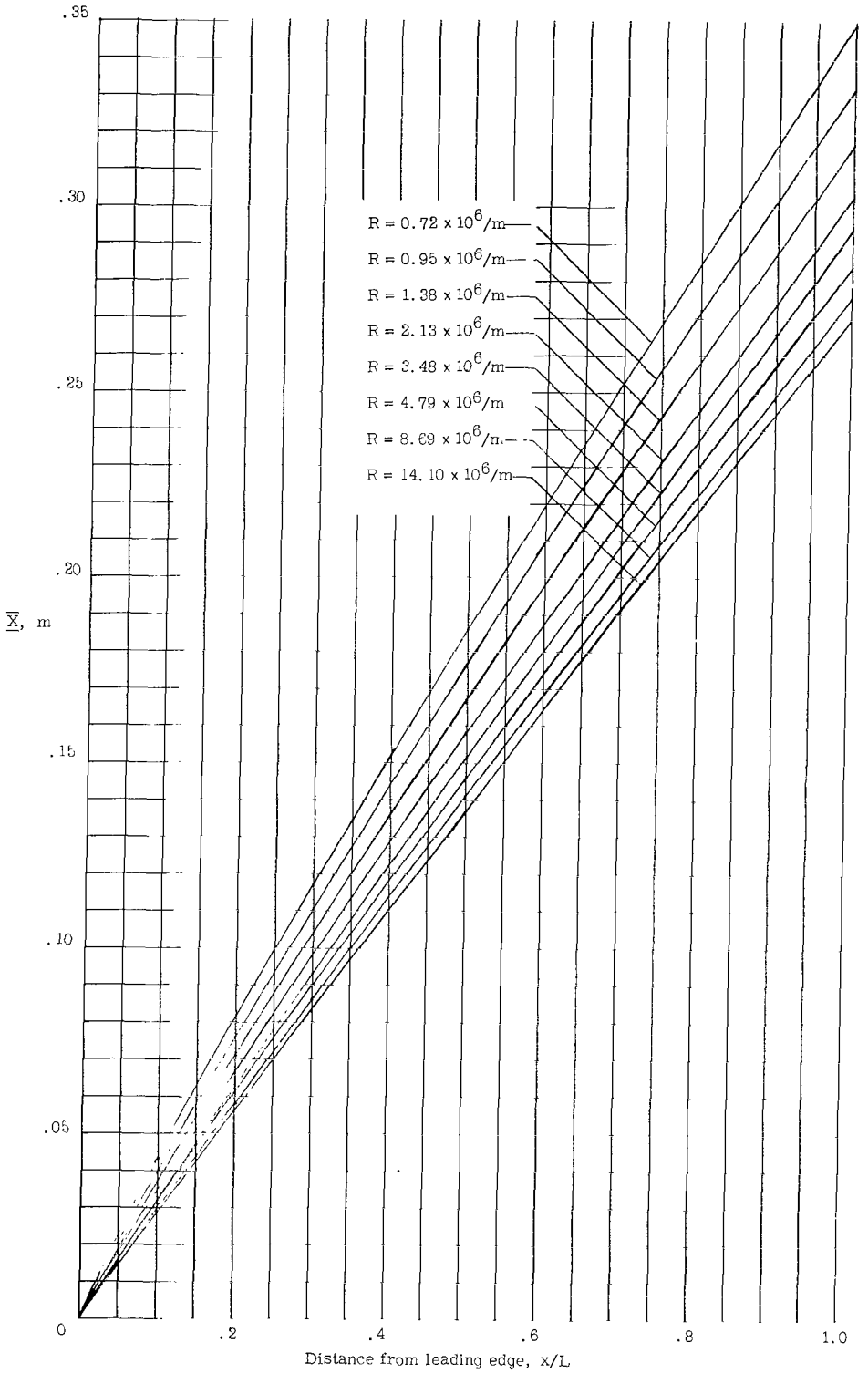

Figure 13.- The x coordinate in the transformed plane for a flat-plate solution at various Reynolds numbers. $T_w/T_t = 0.48$.

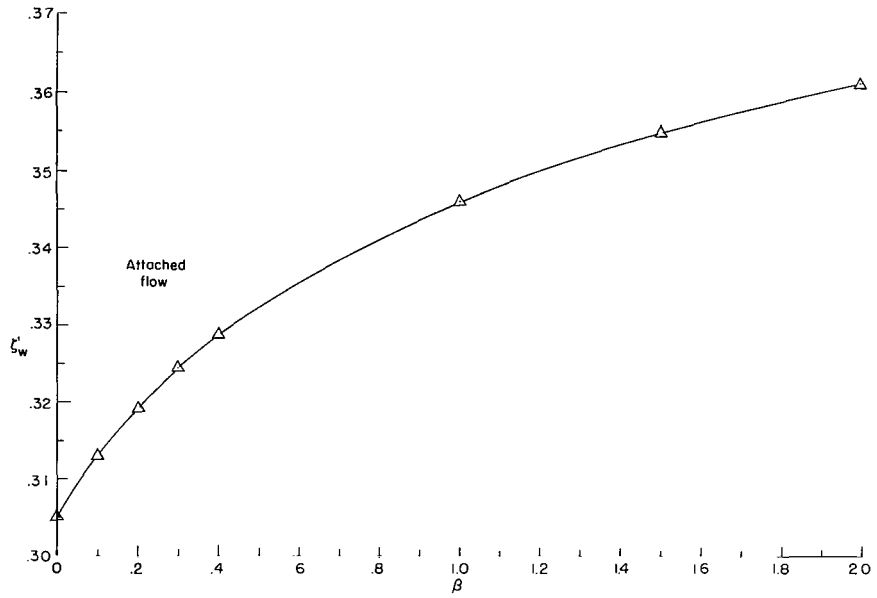

(a) Favorable pressure gradient.

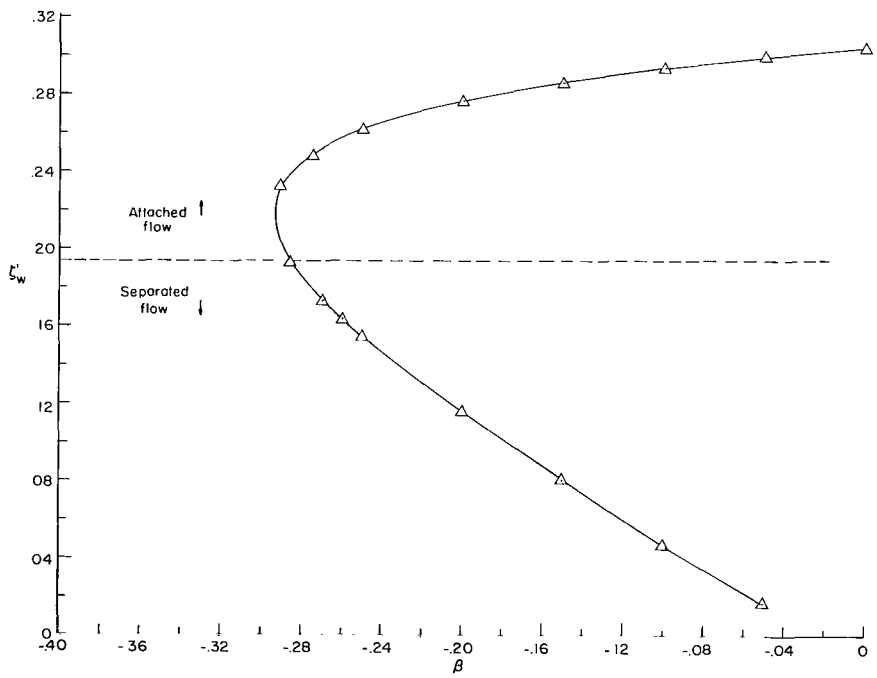

(b) Adverse pressure gradient.

Figure 14.- Similar solution of the heat-transfer parameter as a function of the pressure-gradient parameter. $N_{Pr} = 1.0$; $\Phi = 1.0$; $T_w/T_t = 0.35$.

"The aeronautical and space activities of the United States shall be conducted so as to contribute . . . to the expansion of human knowledge of phenomena in the atmosphere and space. The Administration shall provide for the widest practicable and appropriate dissemination of information concerning its activities and the results thereof."

—NATIONAL AERONAUTICS AND SPACE ACT OF 1958

NASA SCIENTIFIC AND TECHNICAL PUBLICATIONS

TECHNICAL REPORTS: Scientific and technical information considered important, complete, and a lasting contribution to existing knowledge.

TECHNICAL NOTES: Information less broad in scope but nevertheless of importance as a contribution to existing knowledge.

TECHNICAL MEMORANDUMS: Information receiving limited distribution because of preliminary data, security classification, or other reasons.

CONTRACTOR REPORTS: Scientific and technical information generated under a NASA contract or grant and considered an important contribution to existing knowledge.

TECHNICAL TRANSLATIONS: Information published in a foreign language considered to merit NASA distribution in English.

SPECIAL PUBLICATIONS: Information derived from or of value to NASA activities. Publications include conference proceedings, monographs, data compilations, handbooks, sourcebooks, and special bibliographies.

TECHNOLOGY UTILIZATION PUBLICATIONS: Information on technology used by NASA that may be of particular interest in commercial and other non-aerospace applications. Publications include Tech Briefs, Technology Utilization Reports and Notes, and Technology Surveys.

Details on the availability of these publications may be obtained from:

SCIENTIFIC AND TECHNICAL INFORMATION DIVISION

NATIONAL AERONAUTICS AND SPACE ADMINISTRATION

Washington, D.C. 20546